UCLA
COMPUTATIONAL AND APPLIED MATHEMATICS

Level Set Based Simulations of Two-Phase Oil-Water Flows in Pipes (Ph.D. Thesis)

Hyeseon Shim

May 2000

CAM Report 00-18

Department of Mathematics
University of California, Los Angeles
Los Angeles, CA. 90095-1555

http://www.math.ucla.edu/applied/cam/index.html

Level Set Based Simulations of Two-Phase Oil-Water Flows in Pipes

Hyeseon Shim

May 25, 2000

Abstract

We simulate the axisymmetric pipeline transportation of oil and water numerically under the assumption that the densities of the two fluids are different and that the viscosity of the oil core is very large. We develop the appropriate equations for core-annular flows using the level set methodology. Our method consists of a finite difference scheme for solving the model equations, and a level set approach for capturing the interface between two liquids (oil and water). A variable density projection method combined with a TVD Runge-Kutta scheme is used to advance the computed solution in time. The simulations succeed in predicting the spatially periodic waves called bamboo waves, which have been observed in the experiments of Bai, Chen and Joseph [1] on up-flow in vertical core flow. In contrast to the stable case, our simulations succeed in cases where the oil breaks up in the water, and then merging occurs. Comparisons are made with other numerical methods and with both theoretical and experimental results.

1 Introduction

Core-annular flow is a pressure-driven flow through a pipe of one fluid at the core and another fluid in the annulus. This arises naturally for fluids with a high ratio of viscosities because higher viscosity material tend to become encapsulated by lower viscosity material. An industrial application is the lubricated pipelining of crude oil by the addition of water. We want to efficiently transport a very viscous liquid which, on its own, would require costly work. However, when the viscous fluid along the wall is replaced by a much less viscous immiscible fluid, in this case water, then the work required for transportation is significantly lowered.

We compare our results to the experimental results of Bai, Chen and Joseph [1]. Their oil density is 0.905 gcm^{-3}, oil viscosity is 6.01 poise, water density is 0.995 gcm^{-3} and water viscosity is 0.01 poise. The waves are axisymmetric and occur in a very robust regime of up-flow, occupying a large area in the up-flow charts shown in Figures 16.1 - 16.4 of Joseph and Renardy [10].

The average length of a bamboo wave decreases monotonically as the oil input is increased for fixed flow rate of water. Disturbed bamboo waves are observed when the driving pressure gradient is relatively large and the flow is fast. They are observed in both up-flow and down-flow. The main difference between up-flow and down-flow is that in down-flow, the driving pressure gradient and gravity act in the same direction, making water the heavier fluid which falls while the buoyancy holds the oil back, while in up-flow, gravity hinders the water and the oil is encouraged to flow upwards. Naturally, if the driving pressure gradient is sufficiently strong and dominant then the difference between up-flow and down-flow vanishes. Thus disturbed bamboo waves are observed in both regimes.

Applications of the level set formulation were used in ([4],[13],[25]) for incompressible fluid flows. They found that it was best, at least close to the front, to keep ϕ as the signed distance from the front to prevent the development of steep or flat gradients in ϕ. This can be done by solving a simple initial value problem for ϕ which leaves the front location unchanged for fixed time.

We will use the level set approach to solve the problem for core-annular flows in 2D for up-flow and down-flow cases. Horizontal case is tested without the gravity.

Chapter 2 summarizes the equations of motions. Chapter 3 summarizes

the numerical formulations for core-annular flows. Chapter 4 discusses the numerical procedure. Chapter 5 shows our results and our figures. Chapter 6 describes future work.

2 Governing Equations of Motion

2.1 The Equations of Motion

Two-fluid flow is modeled with the Navier-Stokes equation:

$$\frac{\partial \boldsymbol{u}}{\partial t} + \boldsymbol{u} \cdot \nabla \boldsymbol{u} = \frac{1}{\rho}(-\nabla P + \nabla \cdot (2\mu S)) + F \tag{1}$$

where ρ is the density, μ the viscosity, S the viscous stress tensor:

$$S_{ij} = \frac{1}{2}(\frac{\partial u_j}{\partial x_i} + \frac{\partial u_i}{\partial x_j}), \tag{2}$$

and F the source term for the momentum equation. In our calculations, the body force F includes the gravity and interfacial tension force. In core-annular flow, the pressure P is decomposed into two parts, $P = -fx + p$, where f is the driving pressure gradient. The velocity field $\boldsymbol{u}$ is subject to the incompressibility constraint:

$$\nabla \cdot \boldsymbol{u} = 0. \tag{3}$$

The two fluids are immiscible. In this paper, Fluid 1 is oil and Fluid 2 is water. Density and viscosity are constant in each phase but may be discontinuous at the interface. We use a level set function ϕ to represent and capture the interface which is being moved by the following equation:

$$\frac{\partial \phi}{\partial t} + \boldsymbol{u} \cdot \nabla \phi = 0. \tag{4}$$

2.2 Axisymmetric Flow Equations

We now simulate the axisymmetric pipeline transportation of oil and water. For axisymmetric flow, there is no flow in the θ - direction and all θ derivatives are identically zero. So we consider only two variables, r the radial direction and x the axial direction. We define the fluid velocity by the vector $\boldsymbol{u} = (u, v)$

where $u = u(r,x)$ is the radial component of velocity and $v = v(r,x)$ is the component in the axial direction. The governing equations for axisymmetric flow are

$$\frac{\partial u}{\partial t} + u\frac{\partial u}{\partial r} + v\frac{\partial u}{\partial x} = \frac{1}{\rho}\left(-\frac{\partial P}{\partial r} + \frac{1}{r}\frac{\partial}{\partial r}\left(r\left(2\mu\frac{\partial u}{\partial r}\right)\right) + \frac{\partial}{\partial x}\left(\mu\left(\frac{\partial v}{\partial r} + \frac{\partial u}{\partial x}\right)\right) - \frac{1}{r}\left(2\mu\frac{u}{r}\right) + \sigma\kappa\delta\left(\phi\right)\phi_r\right) \tag{5}$$

$$\frac{\partial v}{\partial t} + u\frac{\partial v}{\partial r} + v\frac{\partial v}{\partial x} = \frac{1}{\rho}\left(-\frac{\partial P}{\partial x} + \frac{1}{r}\frac{\partial}{\partial r}\left(r\mu\left(\frac{\partial v}{\partial r} + \frac{\partial u}{\partial x}\right)\right) + \frac{\partial}{\partial x}\left(2\mu\frac{\partial v}{\partial x}\right) + \sigma\kappa\delta(\phi)\phi_x\right) + g \tag{6}$$

and the incompressibility constraint is

$$\frac{1}{r}\left(\frac{\partial(ru)}{\partial r}\right) + \frac{\partial v}{\partial x} = 0. \tag{7}$$

2.3 Parameters for Equations

In dimensional terms in core-annular flow, the pipe radius is denoted by R_2, the base velocity is $\boldsymbol{u} = (0, V_i(r)), i = 1, 2$, and the interface position is $r = R_1$, where $P_2 - P_1 = \sigma/R_1$ and σ is the interfacial tension. The pressure gradient in the axial direction is a constant. Also, $dP/dx = -f$. There are four dimensionless parameters :

$$m = \mu_2/\mu_1,\ a = R_2/R_1,\ \zeta = \rho_2/\rho_1,\ K = (f + \rho_1 g)/(f + \rho_2 g), \tag{8}$$

where K measures the ratio of driving forces in the core and annulus. We choose the centerline velocity to be

$$V_0(0) = (f + \rho_2 g)\frac{R_1^2}{4\mu_2}A, \quad where\ A = mK + a^2 - 1 + 2(K-1)\log a. \tag{9}$$

The dimensionless base velocity field is $(0, V(r))$ where

$$V(r) = \begin{cases} \frac{1}{A}(a^2 - r^2 - 2(K-1)log(r/a)) & 1 \le r \le a, \\ 1 - \frac{1}{A}(mr^2K) & r < 1. \end{cases} \tag{10}$$

The interfacial tension parameter is $J = \sigma R_1 \rho_1 / \mu_1^2$ and the Reynolds numbers Re_i are defined by $Re_i = \rho_i V_0(0) R_1 / \mu_i, i = 1, 2$, where $Re_1/Re_2 = m/\zeta$. For our numerical simulation, we choose some initial data corresponding to the following parameters:

$$\phi(\boldsymbol{x}(r, x)) = A(0) * \cos(\beta * x) + R_1 \tag{11}$$

where A(0) is the amplitude, β the periodicity, and R_1 the interface position.

3 Numerical Formulation

3.1 Level Set Function

We construct a level set function ϕ such that the interface between two different fluids is the zero level set of ϕ. We initialize ϕ to be the signed distance from the interface using the re-distance algorithm of [19]. So the interface is given by

$$\Gamma = \{\boldsymbol{x} | \phi(\boldsymbol{x}, t) = 0\}. \tag{12}$$

We take $\phi < 0$ in the oil region and $\phi > 0$ in the water region. Therefore we have

$$\phi(\boldsymbol{x}, t) \begin{cases} < 0, & \text{if } \boldsymbol{x} \in \text{oil} \\ = 0, & \text{if } \boldsymbol{x} \in \Gamma \\ > 0, & \text{if } \boldsymbol{x} \in \text{water.} \end{cases} \tag{13}$$

Now we let

$$\boldsymbol{u} = \begin{cases} \boldsymbol{u}_{oil} & \text{if } \phi \leq 0 \\ \boldsymbol{u}_{water} & \text{if } \phi > 0 \end{cases} \tag{14}$$

where $\boldsymbol{u}$ is the fluid velocity. The idea of the level set method is to move ϕ with the correct speed $\boldsymbol{u}$ at the front using the following differential equation:

$$\phi_t + \boldsymbol{u} \cdot \nabla \phi = 0. \tag{15}$$

We must reinitialize, using the simple algorithm developed in [26] to keep ϕ as the signed distance, at least near the front. Additionally, we save computational time by performing these calculations only near the front. There

are several localization algorithms available; we use the relatively simple algorithm developed in [21]. We can rewrite the variables by using the level set function ϕ . The unit normal on the interface, drawn from the oil into the water, is

$$\boldsymbol{n} = \frac{\nabla\phi}{|\nabla\phi|} \tag{16}$$

and the curvature of the interface is

$$\kappa = \nabla \cdot \frac{\nabla\phi}{|\nabla\phi|}. \tag{17}$$

Since the density and viscosity are constant in each region, they take on two different values depending on the sign of ϕ, and we can write

$$\rho(\phi) = \rho_{oil} + (\rho_{water} - \rho_{oil})H(\phi) \tag{18}$$

and

$$\mu(\phi) = \mu_{oil} + (\mu_{water} - \mu_{oil})H(\phi) \tag{19}$$

where $H(\phi)$ is the Heaviside function given by

$$H(\phi) = \begin{cases} 0 & \text{if } \phi < 0 \\ \frac{1}{2} & \text{if } \phi = 0 \\ 1 & \text{if } \phi > 0. \end{cases} \tag{20}$$

The fact that the surface tension can be written as a delta function at the interface has been used by Unverdi & Tryggvason [27], and Brackbill, Kothe & Zemach [3]. The form we use here is due to Chang, Hou, Merriman & Osher [4].

3.2 Dimensionless Form

It is convenient to use the dimensionless form of (5). We use the following six dimensionless variables

$$\begin{gathered} \boldsymbol{x} = R\boldsymbol{x}^* \qquad \boldsymbol{u} = V_0\boldsymbol{u}^* \quad t = (R/V_0)t^* \\ P = P^*\rho_{oil}(V_0)^2 \quad \rho = \rho_{oil}\rho^* \qquad \mu = \mu_{oil}\mu^* \end{gathered} \tag{21}$$

where the superscripts $*$ denote dimensionless variables, R is the undisturbed interface position and V_0 is the centerline velocity. Substituting the above dimensionless variables into (5) and dropping the $*$, we have

$$\frac{\partial u}{\partial t}+u\frac{\partial u}{\partial r}+v\frac{\partial u}{\partial x} = \frac{1}{\rho}\left(-\frac{\partial P}{\partial r}+\frac{1}{Re}\left(\frac{1}{r}\frac{\partial}{\partial r}\left(2\mu r\frac{\partial u}{\partial r}\right)+\frac{\partial}{\partial x}\left(\mu\left(\frac{\partial v}{\partial r}+\frac{\partial u}{\partial x}\right)\right)\right.\right. \\ \left.\left.-2\frac{u}{r^2}\right)+\frac{1}{We}\kappa\delta(\phi)\frac{\partial\phi}{\partial r}\right) \tag{22}$$

$$\frac{\partial v}{\partial t}+u\frac{\partial v}{\partial r}+v\frac{\partial v}{\partial x} = \frac{1}{\rho}\left(-\frac{\partial P}{\partial x}+\frac{1}{Re}\left(\frac{1}{r}\frac{\partial}{\partial r}\left(r\mu\left(\frac{\partial v}{\partial r}+\frac{\partial u}{\partial x}\right)\right)+\frac{\partial}{\partial x}\left(2\mu\frac{\partial v}{\partial x}\right)\right)\right. \\ \left.+\frac{1}{We}\kappa\delta(\phi)\frac{\partial\phi}{\partial x}\right)+\frac{R}{V_0^2}\boldsymbol{g} \tag{23}$$

where the Reynolds number $Re=\frac{\rho_{oil}RV_0}{\mu_{oil}}$, the Weber number $We=\frac{\rho_{oil}RV_0^2}{\sigma}$. Now the density and viscosity, respectively, are

$$\rho(\phi)=\eta+(1-\eta)H(\phi) \tag{24}$$

$$\mu(\phi)=\gamma+(1-\gamma)H(\phi) \tag{25}$$

where $\eta=\rho_{oil}/\rho_{water}$ and $\gamma=\mu_{oil}/\mu_{water}$ are the density ratio and the viscosity ratio, respectively.

3.3 Projection Method

This method was proposed independently by Chorin [5] (1968) and by Temam (1969), while an explicit version of such a method was presented by Fortin et al. (1971). This explicit method is a fractional step method with first-order accuracy in time. At the first step, we compute explicitly a provisional value $\boldsymbol{u}^*$ with

$$\frac{\boldsymbol{u}^*-\boldsymbol{u}^n}{\Delta t}=L(\boldsymbol{u}^n) \tag{26}$$

which is the momentum equation without a pressure gradient. Note that only the discretization in time is considered here. Then, at the second step, we correct $\boldsymbol{u}^*$ by considering the equations:

$$\frac{\boldsymbol{u}^{n+1}-\boldsymbol{u}^*}{\Delta t}=\frac{1}{\rho}(-\nabla P) \tag{27}$$

$$\nabla \cdot \boldsymbol{u}^{n+1} = 0. \tag{28}$$

By taking the divergence of Eq. (27) and by making use of (28), which states that $\boldsymbol{u}^{n+1}$ must be a divergence-free vector, we get the Poisson equation

$$\frac{1}{\Delta t}\nabla \cdot \boldsymbol{u}^* = \nabla \cdot (\frac{1}{\rho}\nabla P). \tag{29}$$

The boundary condition for P is obtained by projecting the vector equation (28) on the outward unit normal $\boldsymbol{n}$ to the boundary Γ. Thus, we obtain the Neumann condition

$$\left(\frac{\partial P}{\partial \boldsymbol{n}}\right)_{\Gamma}^{n+1} = -\frac{1}{\Delta t}(\boldsymbol{u}_{\Gamma}^{n+1} - \boldsymbol{u}_{\Gamma}^*) \cdot \boldsymbol{n} \tag{30}$$

where $\boldsymbol{u}_{\Gamma}^*$ is the (not yet defined) value of $\boldsymbol{u}^*$ on Γ. The condition of compatibility for the Neumann problem is

$$\frac{1}{\Delta t}\int \nabla \cdot \boldsymbol{u}^* ds = -\frac{1}{\Delta t}\int_{\Gamma} (\boldsymbol{u}^{n+1} - \boldsymbol{u}^*) \cdot \boldsymbol{n} ds \tag{31}$$

and it identically satisfies the condition $\int_{\Gamma} \boldsymbol{u}_{\Gamma} \cdot \boldsymbol{n} ds = 0$ which expresses the fact that the velocity on the boundary Γ has a zero total flux. It is important that the discretization with respect to space satisfies the above compatibility condition.

3.4 Thickness of the Interface

To reduce the numerical difficulties presented by the Dirac delta function, we shall give the interface a fixed thickness that is proportional to the spatial mesh size. We replace $\rho(\phi)$ in equation (1) by a smoothed density function which we denote as $\rho_\alpha(\phi)$ and is given by

$$\rho_\alpha(\phi) = \eta + (1 - \eta)H_\alpha(\phi) \tag{32}$$

where

$$H_\alpha(\phi) = \begin{cases} 1 & \text{if } \phi > \alpha \\ 0 & \text{if } \phi < \alpha \\ \frac{1}{2}(1 + \frac{\phi}{\alpha} + \frac{1}{\pi} sin(\frac{\pi x}{\alpha})) & \text{otherwise.} \end{cases} \tag{33}$$

The smoothed delta function is

$$\delta_\alpha(\phi) = \begin{cases} \frac{1}{2\alpha}(1 + cos(\frac{\pi\phi}{\alpha})) & \text{if } |\phi| < \alpha \\ 0 & \text{otherwise} \end{cases} \tag{34}$$

where α is the prescribed "thickness" of the interface (usually $1.5\Delta x$ in our calculations).

4 Numerical Procedure

We now describe the numerical discretization of the equations derived in the previous section. The outline of our scheme is as follows:
Given ϕ^n, defined at cells, and $\boldsymbol{u}^n$, defined at cell centers, we solve for $\phi^{n+1}, \boldsymbol{u}^{n+1}$.

For each time step:

Step 1. Initialize ϕ ($\boldsymbol{x}$,t) such that ϕ is a signed distance function to the front.

Step 2. Solve the governing equation (1) and get the velocity $\boldsymbol{u}^{n+1}$.

Step 3. Update the level set function ϕ^n to ϕ^{n+1} .

Step 4. Reinitialize ϕ .

4.1 Solving the Governing Equations

4.1.1 Spatial Derivatives

We compute $L(\boldsymbol{u}^n)$ and $\boldsymbol{u} \cdot \nabla\phi$ using high order ENO upwind scheme for the convective terms and central differencing for the viscous and curvature terms.

4.1.2 Convection Terms

The convection terms in (1) are discretized as:

$$\boldsymbol{u} \cdot \nabla\phi = \frac{u_{i,j}(\phi_{i+1/2,j} - \phi_{i-1/2,j})}{\Delta r} + \frac{v_{i,j}(\phi_{i,j+1/2} - \phi_{i,j-1/2})}{\Delta x} \tag{35}$$

$$\boldsymbol{u} \cdot \nabla\boldsymbol{u} = \frac{u_{i,j}(\boldsymbol{u}_{i+1/2,j} - \boldsymbol{u}_{i-1/2,j})}{\Delta r} + \frac{v_{i,j}(\boldsymbol{u}_{i,j+1/2} - \boldsymbol{u}_{i,j-1/2})}{\Delta x} \tag{36}$$

where $\phi_{i+1/2,j}$ and $\boldsymbol{u}_{i+1/2,j}$ are calculated by high order ENO scheme.

4.1.3 Viscous and Curvature Terms

We use central differencing for computing the viscous and curvature terms. For the discretization of the divergence of the stress tensor $2\mu D$, we have:

$$\begin{aligned}\nabla \cdot (2\mu D) &= \begin{pmatrix} \frac{1}{r}\frac{\partial}{\partial r}(r(2\mu\frac{\partial u}{\partial r})) + \frac{\partial}{\partial x}(\mu(\frac{\partial v}{\partial r} + \frac{\partial u}{\partial x})) - \frac{1}{r}(2\mu\frac{u}{r}) \\ \frac{1}{r}\frac{\partial}{\partial r}(r\mu(\frac{\partial v}{\partial r} + \frac{\partial u}{\partial x})) + \frac{\partial}{\partial x}(2\mu\frac{\partial v}{\partial x}) \end{pmatrix}_{i,j} \\ &= \begin{pmatrix} \frac{1}{r}D_r(r(2\mu D_r u)) + D_x(\mu(D_r v + D_x u)) - \frac{1}{r}(2\mu\frac{u}{r}) \\ \frac{1}{r}D_r(r\mu(D_r v + D_x u)) + D_x(2\mu D_x v) \end{pmatrix}_{i,j}\end{aligned} \tag{37}$$

where the difference operators are defined as:
For the u-direction case,

$$\begin{aligned} D_r f_{i,j} &= (f_{i+1/2,j} - f_{i-1/2,j})/\Delta r \\ D_r f_{i+1/2,j} &= (f_{i+1,j} - f_{i,j})/\Delta r \\ D_x f_{i,j} &= (f_{i,j+1/2} - f_{i,j-1/2})/\Delta x \\ D_x f_{i,j+1/2} &= (f_{i,j+1} - f_{i,j})/\Delta x \\ \mu_{i+1/2,j} &= \mu(i,j), \quad \mu_{i-1/2,j} = \mu(i-1,j) \\ \mu_{i,j} &= \frac{1}{2}(\mu(i,j) + \mu(i-1,j)) \\ \mu_{i,j+1/2} &= \frac{1}{4}(\mu(i-1,j) + \mu(i,j) + \mu(i-1,j+1) + \mu(i,j+1)) \end{aligned}$$

$$\begin{aligned} \mu_{i,j-1/2} &= \frac{1}{4}(\mu(i-1,j-1) + \mu(i,j-1) + \mu(i-1,j) + \mu(i,j)) \\ v_{i+1/2,j+1/2} &= v(i,j+1), \; v_{i-1/2,j+1/2} = v(i-1,j+1) \\ v_{i+1/2,j-1/2} &= v(i,j), \quad v_{i-1/2,j-1/2} = v(i-1,j) \\ r_{i,j} &= \frac{1}{2}(r(i,j) + r(i-1,j)). \end{aligned}$$

The v-direction case is calculated similarly. For discretization of the curvature $\kappa(\phi) = \nabla \cdot \frac{\nabla\phi}{|\nabla\phi|}$, we have:

$$\kappa(\phi) = \frac{1}{r}\frac{\partial}{\partial r}\left(r\frac{\frac{\partial\phi}{\partial r}}{|\nabla\phi|}\right) + \frac{\partial}{\partial x}\left(\frac{\frac{\partial\phi}{\partial x}}{|\nabla\phi|}\right) \tag{38}$$

$$|\nabla\phi| = \sqrt{\left(\frac{\partial\phi}{\partial r}\right)^2 + \left(\frac{\partial\phi}{\partial x}\right)^2}. \tag{39}$$

4.1.4 Surface Tension

The surface tension is prescribed as

$$\frac{1}{We}\frac{\kappa(\phi)\delta(\phi)\nabla\phi}{\rho}. \tag{40}$$

The discretization of the surface tension at cell (i,j) is

$$[\kappa(\phi)\delta(\phi)\phi_r]_{i,j} = \kappa(\phi)_{i,j}\delta(\phi)_{i,j}(\phi_r)_{i,j} \tag{41}$$

where

$$\begin{aligned}
\kappa_{i,j} &= \frac{1}{2}(\kappa(i,j)+\kappa(i-1,j)) \\
\delta(\phi)_{i,j} &= \frac{1}{2}(\delta(\phi(i,j))+\delta(\phi(i-1,j))) \\
(\phi_r)_{i,j} &= \frac{\phi_{i+1/2,j}-\phi_{i-1/2,j}}{\Delta r} \\
&= \frac{\phi(i,j)-\phi(i-1,j)}{\Delta r} \\
\rho_{i,j} &= \frac{1}{2}(\rho(i,j)+\rho(i-1,j)).
\end{aligned}$$

4.2 Semi-Implicit Method for Viscosity Term

4.2.1 Semi-Implicit Scheme

We use an unconditionally stable method for the viscous terms in two- dimensional flow [14], which is applied in the following way to our axisymmetric case:

$$\begin{aligned}
\frac{\partial u}{\partial t}+u\frac{\partial u}{\partial r}+v\frac{\partial u}{\partial x} &= \frac{1}{\rho}\left(-\frac{\partial P}{\partial r}+\frac{1}{r}\frac{\partial}{\partial r}\left(r\left(2\mu\frac{\partial u}{\partial r}\right)\right)+\frac{\partial}{\partial x}\left(\mu\left(\frac{\partial v}{\partial r}+\frac{\partial u}{\partial x}\right)\right)\right. \\
&\quad \left.-\frac{1}{r}\left(2\mu\frac{u}{r}\right)+\sigma\kappa\delta(\phi)\phi_r\right)
\end{aligned} \tag{42}$$

$$\begin{aligned}
\frac{\partial v}{\partial t}+u\frac{\partial v}{\partial r}+v\frac{\partial v}{\partial x} &= \frac{1}{\rho}\left(-\frac{\partial P}{\partial x}+\underbrace{\frac{1}{r}\frac{\partial}{\partial r}\left(r\mu\left(\frac{\partial v}{\partial r}+\frac{\partial u}{\partial x}\right)\right)}_{I}+\frac{\partial}{\partial x}\left(2\mu\frac{\partial v}{\partial x}\right)\right. \\
&\quad \left.+\sigma\kappa\delta(\phi)\phi_x\right)+g.
\end{aligned} \tag{43}$$

Here, we need to change the I-term to the following form:

$$I = \frac{1}{r}\frac{\partial}{\partial r}\left(r\mu\left(\frac{\partial v}{\partial r}\right)\right) + \frac{\mu}{r}\frac{\partial u}{\partial x} + \frac{\partial}{\partial r}\left(\mu\frac{\partial u}{\partial x}\right). \tag{44}$$

So we have the following semi-implicit formations:

$$\begin{aligned}\rho\frac{u^* - u^n}{\Delta t} &= \frac{1}{r}\frac{\partial}{\partial r}\left(r\left(2\mu\frac{\partial u^*}{\partial r}\right)\right) + \frac{\partial}{\partial x}\left(\mu\left(\frac{\partial v^n}{\partial r} + \frac{\partial u^*}{\partial x}\right)\right) \\ &\quad -2\mu\frac{u^*}{r^2} + explicit - terms,\end{aligned} \tag{45}$$

$$\begin{aligned}\rho\frac{v^* - v^n}{\Delta t} &= \frac{1}{r}\frac{\partial}{\partial r}\left(r\mu\left(\frac{\partial v^*}{\partial r}\right)\right) + \frac{\partial}{\partial r}\left(\mu\frac{\partial u^n}{\partial x}\right) + \frac{\mu}{r}\frac{\partial u^*}{\partial x} \\ &\quad +\frac{\partial}{\partial x}\left(2\mu\frac{\partial v^*}{\partial x}\right) + explicit - terms,\end{aligned} \tag{46}$$

where the inertial terms are treated as explicit terms. Here u^* depends on v^n only explicitly but v^* is coupled to u^* implicitly. From equation (45) we solve for u^* first. Next, we substitute u^* in the right side of equation (46) and solve for v^*.

4.2.2 Factorization

We adapted the factorization technique in [15] to our scheme so we need only solve a tridiagonal system and the error of factorization is of order $O(\Delta t^3)$. This semi-implicit scheme reduces our computing time. The equation (4.11) can be expressed as

$$\left\{I - \frac{\Delta t}{\rho}\left[\frac{1}{r}\frac{\partial}{\partial r}\left(2\mu\frac{\partial}{\partial r}\right) + \frac{\partial}{\partial x}\left(\mu\frac{\partial}{\partial x}\right) - 2\mu\frac{1}{r^2}\right]\right\}u^* = explicit - terms, \tag{47}$$

and the equation (4.12) can be expressed as

$$\left\{I - \frac{\Delta t}{\rho}\left[\frac{\partial}{\partial r}\left(r\mu\frac{\partial}{\partial r}\right) + \frac{\partial}{\partial x}\left(2\mu\frac{\partial}{\partial x}\right)\right]\right\}v^* = explicit - terms. \tag{48}$$

As the full explicit scheme, this semi-implicit scheme is first order in precision. Although it is easier to solve than the coupled system, it still requires

inversions of a large sparse matrix. We applied a factorization technique to the left-hand sides of equations (47) and (48):

$$\left\{I - \frac{\Delta t}{\rho}\left[\frac{1}{r}\frac{\partial}{\partial r}\left(2\mu\frac{\partial}{\partial r}\right)\right]\right\}\left\{I - \frac{\Delta t}{\rho}\left[\frac{\partial}{\partial x}\left(\mu\frac{\partial}{\partial x}\right)\right]\right\}$$

$$\left\{I + \frac{\Delta t}{\rho}\left[2\mu\left(\frac{1}{r^2}\right)\right]\right\}u^* = explicit - terms, \tag{49}$$

$$\left\{I - \frac{\Delta t}{\rho}\left[\frac{\partial}{\partial r}\left(r\mu\frac{\partial}{\partial r}\right)\right]\right\}\left\{I - \frac{\Delta t}{\rho}\left[\frac{\partial}{\partial x}\left(2\mu\frac{\partial}{\partial x}\right)\right]\right\}v^* = explicit - terms. \tag{50}$$

The inversion of the left-hand side of equations (49), (50) requires solving only tridiagonal matrices; this results in a significant reduction in computation. In fact, the solution of these tridiagonal systems can be done in only $O(N)$ operations (where N is the number of grid points) and is insignificant compared to the complexity for obtaining the solution of the pressure equation.

4.2.3 Stiffness of Viscosity

The viscosity of oil is very different from that of water while the densities are similar. The Reynolds number for the water annulus is roughly 600 times that of the core oil. So the large Reynolds number in the water and the much smaller Reynolds number in the oil impose severe restrictions on the time step size, according to the stability criteria for the explicit formulation. This suggests the method of implementation for the viscous terms.

4.3 Solving the Pressure Term

We use the PCG(preconditioned conjugate gradient) method with Incomplete Cholesky Decomposition as a preconditioner to solve the resulting Poisson equation for the pressure:

$$\nabla \cdot (\frac{1}{\rho}\nabla P) = \nabla \cdot \boldsymbol{u}^* \tag{51}$$

$$\frac{1}{r}\frac{\partial}{\partial r}\left(\frac{r}{\rho}P_r\right) + \frac{\partial}{\partial x}\left(\frac{1}{\rho}P_x\right) = \frac{1}{\Delta t}\left(\frac{1}{r}\frac{\partial}{\partial r}(ru^*) + \frac{\partial v^*}{\partial x}\right) \tag{52}$$

Then multiplying by r on both sides to make a symmetric system,

$$\frac{\partial}{\partial r}\left(\frac{r}{\rho}P_r\right)+\frac{\partial}{\partial x}\left(\frac{r}{\rho}P_x\right)=\frac{1}{\Delta t}\left(\frac{\partial}{\partial r}(ru^*)+\frac{\partial}{\partial x}(rv^*)\right). \tag{53}$$

For the left hand side of the equation, we use the following discretization:

$$\frac{\partial}{\partial r}(\frac{r}{\rho}P_r)_{i,j}=\frac{\frac{r_{i+1/2,j}}{\rho_{i+1/2,j}}(P_{i+1,j}-P_{i,j})-\frac{r_{i-1/2,j}}{\rho_{i-1/2,j}}(P_{i,j}-P_{i-1,j})}{\Delta r^2} \tag{54}$$

where

$$\begin{aligned}
r_{i+1/2,j} &= \frac{1}{2}(r(i+1,j)+r(i,j)) \\
r_{i-1/2,j} &= \frac{1}{2}(r(i,j)+r(i-1,j)) \\
\\
\rho_{i+1/2,j} &= \frac{1}{2}(\rho(i+1,j)+\rho(i,j)) \\
\rho_{i-1/2,j} &= \frac{1}{2}(\rho(i,j)+\rho(i-1,j)) \\
P_{i+1,j} &= P(i+1,j) \\
P_{i,j} &= P(i,j) \\
P_{i-1,j} &= P(i-1,j).
\end{aligned}$$

For the right hand side of the equation, we adapt the same discretization. In the above calculation, we are using the average value for r and ρ.

4.4 Time Step Restriction

The timestep Δt is determined by restrictions due to the convection, gravity, viscosity and surface tension. The convective time step restriction is given by

$$\Delta t\ dt_c=\Delta t\left(\frac{|u|_{max}}{\Delta r}+\frac{|v|_{max}}{\Delta x}\right)\leq 1 \tag{55}$$

where $|u|_{max}$ and $|v|_{max}$ are the maximum magnitudes of the velocities. The viscous time step restriction is given by

$$\Delta t\ dt_v=\Delta t\left(max\{\frac{\mu_{oil}}{\rho_{oil}},\frac{\mu_{water}}{\rho_{water}}\}\left(\frac{2}{\Delta r^2+\Delta x^2}\right)\right)\leq 1 \tag{56}$$

where the "max" function returns as the maximum value of its arguments. Gravity can be included in the convection estimation. Note that $|v|_{max}+|g|\Delta t$ is a linear approximation to a bound on the velocity in the vertical direction due to the effects of gravity at the end of a time step. Then $\Delta t(\frac{|v|_{max}+|g|\Delta t}{\Delta x}) \leq 1$ changes to

$$\Delta t \left(\frac{-|v|_{max} + \sqrt{|v|^2_{max} + 4|g|\Delta y}}{2|g|} \right) \leq 1 \tag{57}$$

or

$$\frac{\Delta t}{2} \left(\frac{|v|_{max}}{\Delta x} + \sqrt{\left(\frac{|v|_{max}}{\Delta x} \right)^2 + \frac{4|g|}{\Delta x}} \right) \leq 1 \tag{58}$$

as a time step restriction for the velocity in the vertical direction. We rewrite (55) and (56) to

$$\frac{\Delta t}{2} \left((dt_c + dt_v) + \sqrt{(dt_c + dt_v)^2 + \frac{4F_r}{\Delta r} + \frac{4F_x}{\Delta x}} \right) \leq 1 \tag{59}$$

where $\boldsymbol{F} = (F_r, F_x)$ is the force due to gravity and surface tension. In the δ-function formulation, $\frac{\sigma\delta\kappa}{\rho}$ is added to the right hand side of the equations for velocity. In the GFM(Ghost Fluid Method)[13], (59) is written as

$$\Delta t \left(\frac{(dt_c + dt_v) + \sqrt{(dt_c + dt_v)^2 + 4(\Delta t_g)^2 + 4(\Delta t_s)^2}}{2} \right) \leq 1 \tag{60}$$

where

$$\Delta t_g = \sqrt{\frac{|g|}{\Delta x}} \tag{61}$$

and

$$\Delta t_s = \sqrt{\frac{\sigma|\kappa|}{min\{\rho_{oil}, \rho_{water}\}(min\{\Delta r, \Delta x\})^2}} \tag{62}$$

represent the time step restrictions due to gravity and surface tension respectively. In our numerical simulations, a CFL restriction of $\frac{1}{2}$ is used.

Therefore,

$$\Delta t \left(\frac{(dt_c + dt_v) + \sqrt{(dt_c + dt_v)^2 + 4(\Delta t_g)^2 + 4(\Delta t_s)^2}}{2} \right) \leq \frac{1}{2} \qquad (63)$$

is used. Due to the factorization technique, we can relax our time step condition by removing the restriction for viscosity term.

4.5 Re-Initialization Operation

It is numerically desirable to keep $\phi(\boldsymbol{x}, t)$ as a signed distance function. In general, it is not always possible to prevent ϕ from deviating away from a signed distance function. One way to reinitialize is to find the location of the front with some interpolation method and compute the signed distance function to this front [19]. This approach has the advantage that it only moves the interface up to the numerical accuracy of the interpolation method but the disadvantage is its high cost and the likelihood of introducing some spurious irregularities into the data. So a smoothing process is usually needed in conjunction with this approach. A more elegant way is suggested in [20], where the following Hamilton- Jacobian equation:

$$\begin{cases} \phi_\tau + S(\phi_0)(|\nabla \phi| - 1) = 0 \\ \phi(\boldsymbol{x}, 0) = \phi_0(\boldsymbol{x}) \end{cases} \qquad (64)$$

is solved to steady state, giving the desired signed distance function. This method converges in a neighborhood of the front. The reason is very simple since ϕ propagates with speed 1 along the characteristics that are normal to the interface, and converges in time ϵ to a signed distance function in a neighborhood of Γ of width ϵ. In [20], the authors approximate $S(\phi)$ by

$$S_\epsilon(\phi) = \frac{\phi}{\sqrt{\phi^2 + \epsilon^2}} \qquad (65)$$

with $\epsilon = \Delta x$, and used a second order ENO scheme [20] to approximate the space derivatives.

5 Results

Our experiments simulate the motions of Core-Annular flow. We numerically simulate up-flow and down-flow cases of the interface in 2D for a vertical pipe

case. Also we add our horizontal simulation of the simple case.

5.1 Numerical Study of Experimental Regime

We suppose that the flow is spatially periodic and determine the wavelength of the waves from experimental data. The reason for assuming periodicity of the flow is that the simulation for nonperiodic flow is not yet possible due to the computational cost, because the pipeline in Bai, Chen and Joseph(1989) is 90 inches, which is very long in comparison with its cross-sectional radius, 0.375 inches.

5.1.1 Example 1

We begin with the case with $[Q_w, Q_o] = [200, 429]\, cm^3 min^{-1}$. In Figure 3, the experimental snap-shot shows the coexistence of waves with different wavenumbers. The experimental hold-up ratio h is 1.39 for this flow and from equation (3.4) in J. Li and Y. Renardy [14], we obtain the corresponding value of $a = 1.28$. The parameters for the corresponding PCAF(Perfect Core-Annular Flow) are first calculated using the fixed values of V_o and a. The superficial oil velocity is $V_o = Q_o/(\pi R_2^2) = 10.34\, cms^{-1}$. Then we can calculate the other parameters of PCAF using equation (18.15) of Joseph & Renardy [10] and other formulas. Now we have the parameters $Re_1 = 0.9498, m = 0.00166, \eta = 1.1, J = 0.07961$ and $K = -0.4552$. We initialize our numerical simulation with a very small perturbation amplitude $A(0) = 0.001$, in order to keep the flow in the linear regime for a relatively long time. Also, we choose the wavenumber $\alpha = 2.0$ for this flow. According to the formula for centerline velocity, we use $V_0^* = 16.9531$. This simulation is carried out on a 50 x 122 mesh over one spatial period on a domain [0, 1.28] x [0, 3.14]. Figure 4 shows our results for this case. We also display the contour of the pressure field corresponding to the interfacial shape.

5.1.2 Example 2

Numerical simulations are performed by initializing with wavenumbers $\alpha =$ 1.5, 1.75, and 2.0, which is the range relevant to the experimental situation. Beyond the linear regime, these core-annular flows evolve into bamboo waves with constant amplitude. Figure 5 shows our wave shapes for the above four wavenumbers in the nonlinear regime.

There is an *adjustment period*, when the interface shape changes from the initial cosine shape to the bamboo shape. The steady solution calculated by Bai, Kelkar and Joseph [2] under solid-core and density-matching assumptions produces an interface shape like the one found in their experiment. However, their interface shape is too rounded and smooth compared to their experimental snap-shot (Figure 3), which shows an almost symmetric form of the crest, with a pointed peak. The crest is slightly sharper at the front and less sharp at its back. The numerical simulation produced by Li and Renardy [14] under the same assumptions that we use established an interface shape with a symmetric form for the crest and a pointed peak. Our result for the same case successfully reproduced these details.

5.1.3 Example 3

The corresponding PCAF base velocity profile is shown in Figure 6. This is a mixed flow, up for oil and water near the oil core, down for water near the pipe wall. Figure 7 shows the base velocity field for PCAF at $Re = 3.0$, $K =$ -0.9993. This is fully up-flow in both fluids. The initial amplitude is chosen as $A(0) = 0.005$.

5.1.4 Example 4

To investigate the flow field in more detail, we examine the contour of the pressure field. We produce the contour for pressure for $Re = 3.0$, $a = 1.28$. In Figure 8, we plot the contour of the pressure field for this example. In the water, the pressure field reaches its maximum value above the crest and its minimum value below the crest. From below the crest to above, the pressure increases monotonically in the water. Thus, the pressure contours are nearly horizontal lines. The pressure field in the oil core is also shown in Figure 8.

5.1.5 Example 5

For the radius ratio $a = 1.28$, the oil core is relatively close to the pipe wall and the interaction between them is strong. In this example, we investigate what happens if the oil core is relatively far away from the pipe wall, so that the water has a large room to stay. Consider the experimental data point # 1 in Figure 2, where $a = 1.61$, $F =$ -1.06699, which correspond to $J = 0.063354$, and $K =$ -2.0303. The centerline velocity for PCAF is $V_0^* = 83.91\ cm/sec$ so our Reynolds number is $Re_1 = 3.73754$. We set the

initial amplitude of perturbation $A(0) = 0.1$. The calculation is carried out on a 50 x 195 mesh over one spatial period on the domain [0, 1.61] x [0, 2.618]. We choose the wavenumber $\alpha = 2.4$ corresponding to a wavelength for this flow. Linear theory indicates that the wavenumber $\alpha = 2.4$ is the most dangerous mode for this case. We display the corresponding interface profiles in Figure 9 at time $t = 0$, 20, 40, 60 and 140. The interface shape at $t = 40$ reveals some asymmetry in the interface crest in that it is narrower than the trough. This can be explained by the fact that the low-viscosity water provides less resistance, making it easier for the high-viscosity oil to penetrate into it.

5.1.6 Example 6

In our numerical simulation for this up-flow case, we select $Re = 3.0$ with $a = 1.28$. The domain is [0, 1.28] x [0, 3.142] with 30 x 120 mesh. The superficial oil velocity V_o is 10, $J = 0.0795$ and K = -0.9993. We test this case for the final time $t = 100$, but starting from $t = 20$, the interfacial shape doesn't change and remains so until the final time.

5.2 Direct Simulation for the Down Flow

5.2.1 Example 1

In down-flow, the pressure and buoyancy forces of oil oppose those of water. This tends to compress, even eliminate bamboo waves and creates the flow type called "disturbed core-annular flow". It was first found in the experiments of Bai, Chen and Joseph [1]. The down-flow with parameters Re = 2.5, $a = 1.7$, $m = 0.00166$, $\eta = 1.1$, $J = 0.06$ and K = -0.542709 was studied by Renardy [23] in the context of non- axisymmetric perturbations. Here, we investigate this flow under the axisymmetric assumption. Numerical investigation of this flow is performed on a 30 x 200 mesh. We set the initial amplitude $A(0) = 0.01$. The asymmetry of the crest is prominent, due to the effect of the buoyancy of oil relative to water, which flattens the back of the crest and steepens the front of the crest. We display our result in Figure 11.

5.2.2 Example 2

In this example, we take a different Reynolds number while keeping the relative driving force K constant as -0.542709. Here, we simulate our test case

with the centerline velocity $V_0(0)^*$ = -28.25547. Since our Reynolds number is 3.0, we use 2.625 as the corresponding wave number. Our calculation is carried over a 30 x 150 mesh on the domain [0, 0.47625] x [0, 2.3936]. Figure 12 shows the sequence of the interface positions at t = 0, 30, 60, 90, 120 and 150.

5.3 Effect of Reynolds number Re and Flow

We run simulations for several different Reynolds numbers in the case of up- and down- flow for a vertical pipe. In Figure 13, we show the results for up-flow cases with various Reynolds numbers. We find that as the Reynolds number increases, the length of the waves is shortened. In Figure 14, we show the down-flow case in the vertical pipe. Just as in the up-flow case, as the Reynolds number increases, the length of the waves is shortened.

5.4 Effect of Wave number α and Flow

The effect of wave number α is tested with the case $Re = 0.94983$. We display the interfacial profiles in Figure 4. According to our results, we conclude that as the wave number increases, the length of waves is shortened. While the wave number α changed, taking the values 1.5, 1.75 and 2.0, we fixed the other parameters to find the relation between α and the flow. We get very good bamboo waves for each wave number case.

5.5 Effect of radius ratio a and Flow

We simulate the CAF using the wave numbers described in Table 1 and Table 2. The results show that as the wave number is increased, the length of the waves is shortened, as expected and as experiments show, since the Reynolds numbers are increased along with the wave numbers.

5.6 Breaking of the Oil Core

Our numerical simulation is performed with the same interface shape as in the other cases. Since there is no big difference between the volume of fluid method and the level set approach for this CAF problem, we consider a special case to take advantage of level set method. As we know, the level set methodology has a great advantage in breaking or merging problems.

5.6.1 Example 1

In this example, we produce the simulation of the breaking of the oil core in Figure 15. We start with the initial amplitude $A(0) = 0.01$ and a cosine interface shape. Given $Re = 1.0$, $a = 1.61$, $J = 0.063354$ and K = -2.030303, we select our wave number $\alpha = 0.9$ and the centerline velocity $V_0^* = 10.03$. Our numerical simulation is performed on a 50 x 216 mesh over the domain [0, 1.61] x [0, 6.98]. It starts to change its topological shape around the dimemsionless time $t = 10$. The lower two fingers grow outward and start to approach the oil core, i.e. merge into the oil core, around $t = 50$. For a moment, inside of the oil core, a water bubble appears and disappears. Since we don't have a fine enough grid for our simulation, this example doesn't display perfect bamboo waves. But we show that the oil keeps the water and carries it for a moment. And it "almost" becomes bamboo wave.

5.6.2 Example 2

Figure 16 is the result of another case of the water in the oil core.

5.6.3 Example 3

We next do a different simulation to see what happens if we change our domain to [-0.47625, 0.47625] x [0, ymax]. We are not changing the assumption for the axisymmetry. At the final time $t = 0.5$, we get a bubble. This topological change is different from the other case, *i.e.* Example 1 in this section displayed in Figure 16. We display the 4 oil bubbles in the vertical pipe for Figure 17.

5.6.4 Example 4

Figure 18 shows the results of numerical simulations for oil bubbles in water. This example shows that in the middle of the adjustment period, several oil bubbles exist in the water, then they merge back into the oil core, and stick to it. The Reynolds number is 3.737354, the ratio of the radius is 1.61 and K, the ratio of driving forces in the core and annulus is -2.030303. We do our simulations on a 50 x 80 mesh on the domain [0, 1.61] x [0, 2.6180].

Re	1.0	1.5	2.0	3.0	3.74
α	0.9	1.18	1.45	1.95	2.4

Table 1: The Reynolds numbers and the corresponding wavenumbers for up-flow, $a = 1.6$, $m = 0.00166$, $\eta = 1.1$, $J = 0.063354$ and K = -2.030303

Re	1.2	2.0	2.5	3.0
α	1.4	1.675	1.975	2.625

Table 2: The Reynolds numbers and the corresponding wavenumbers for down-flow, $a = 1.7$, $m = 0.00166$, $\eta = 1.1$, $J = 0.063354$ and K = -0.542709

5.7 Horizontal Flow without Gravity

Finally, we apply the level set method to simulate the horizontal flow case of CAF. Without the axisymmetric property the numerical simulation fails because the buoyancy of the oil makes the oil move upwards and at the same time, water needs to move to give room to the oil but there is no room for the water. To do this we require axisymmetry for our numerical simulations. Thus, we ignore the effect of gravity. The pressure gradient needs to be big enough to move the fluid from left to right. We choose $Re = 3.7$ and find the corresponding parameters. The initial shape is a cosine graph with amplitude $A(0) = 0.01$. This gives a very smooth interface. Figure 19 shows the result of this computation.

5.8 CPU times and Figures

We use Table 1 and Table 2 to give the Reynolds numbers and corresponding wave numbers for up-flow and down-flow. We describe our CPU times for our figures in Table 3 and Table 4. At the same time, we tabulate CPU times which we used factorization in Tables 3 and 4.

Re	CPU time without Factorization	CPU time with Factorization
1.2	1 month	1 week
2.0	3 weeks	5 days
2.5	2 weeks	3 days
3.0	1 week	1 day

Table 3: The Reynolds numbers and CPU times for down-flows

Re	CPU time without Factorization	CPU time with Factorization
1.0	1 month	1 week
1.5	3.5 weeks	5 days
2.0	3 weeks	3 days
3.0	2 weeks	2 days
3.7	1 week	1 day

Table 4: The Reynolds numbers and CPU times for up-flows

6 Summary

6.1 Conclusion

Core-annular flows of liquids with different density and a high viscosity ratio were computed in a direct numerical simulation using the level set method. It was assumed that the flow is axisymmetric and periodic. These assumptions reduce the computational cost. In dimensional terms, for given material parameters, we obtain solutions when the volume flow rates of oil, water and the hold-up ratio are prescribed. Our simulation with the level set method on core-annular flow represents an improvement over the results of Bai, Chen and Joseph [1] , who solved for the steady solution of the governing equations assuming the densities matched and assuming a solid core, and on the results of Li and Renardy [14], who investigated this problem with different densities for two liquids. In contrast with Li and Renardy's work, we reduced the computational time without using factorization. Furthermore, we investigated the case where the oil core breaks into water, forming a separate bubble there. This was easy to handle due to the level set methodology.

6.2 Future Work

We intend to simulate realistic core-annular flow in the horizontal case. We assumed axisymmetric flow to reduce the computational cost, so we were forced to remove the gravitational force in the present work. For some of our cases, we had high computational costs. We hope to implement a more efficient method to reduce these costs.

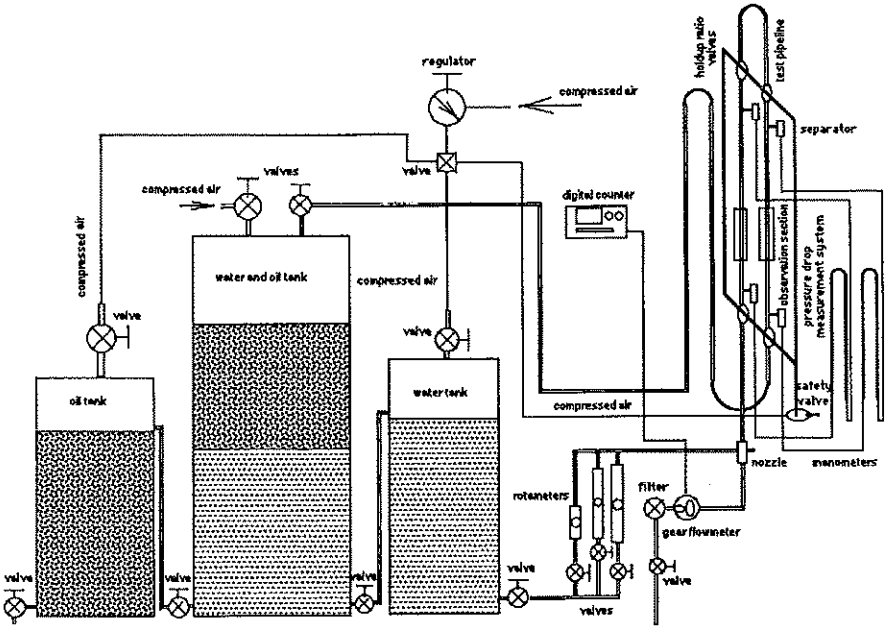

Figure 1: [Bai, Chen and Joseph, 1992] Experimental system. The pipeline is a $\bigcap$ loop which is mounted on the wall with its long legs vertical, aligned with gravity. The flow of oil and water to the pipeline is established by the pressure of compressed air in the oil and water tanks.

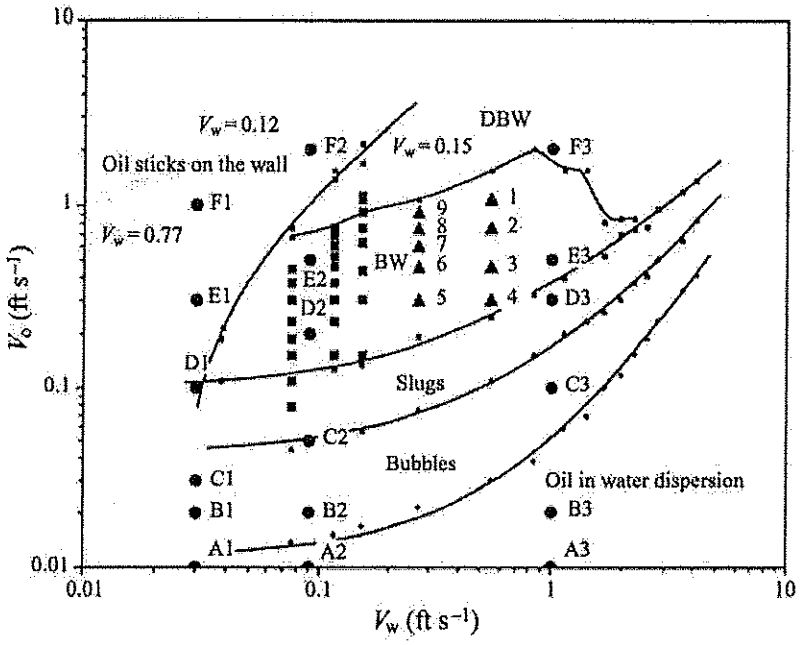

Figure 2: [Bai, Chen and Joseph, 1992] This flow chart displays the types of flow that arise in up-flow as function of the superficial oil velocity V_o and the superficial water velocity V_w.

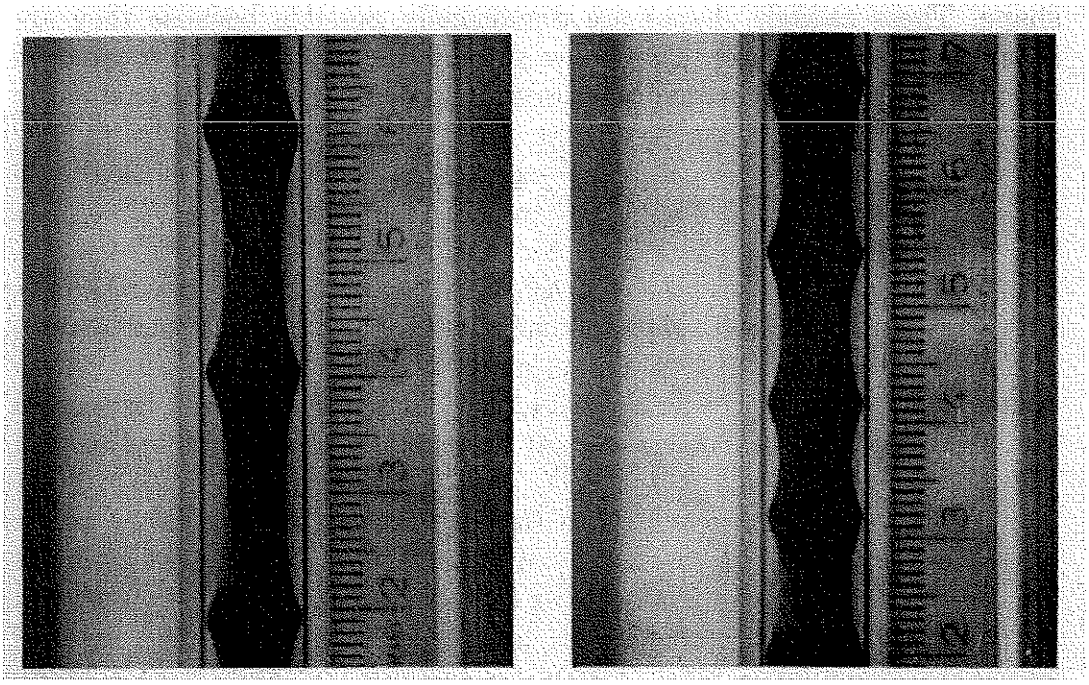

Figure 3: [Bai, Chen and Joseph, 1992] Thin and thick bamboo waves. The bamboo thickens and the average length of a wave decreases when the oil velocity increases at a fixed value of the water velocity.

A Notations

a = R_2/R_1 radius ratio

A = area of the pipe (πR_2^2
where $R_2 = 3/16$ inches is the inside radius of the pipe)

η = $R_1/R_2 = 1/a$ radius ratio

$\boldsymbol{g}$ = gravity constant 980 $cm/(s^2)$

J^* = $\rho_o \sigma R_2/\mu_o^2$

J = J^*/a interfacial tension parameter

L = pipe length

m = μ_2/μ_1 viscosity ratio (oil inside corresponds to $m < 1$)
In the experiments $m = 1/601$ at 22^oC

μ_1 = μ_o oil viscosity

μ_2 = μ_w water viscosity

f^* = constant pressure gradient

Q_1 = Q_o volume flow rate of oil

Q_2 = Q_w volume flow rate of water

R_1 = mean radius of the core

R_2 = mean radius of the pipe

Re = Reynolds number

ρ_1 = ρ_o oil density

ρ_2 = ρ_w water density

σ = interfacial tension

$V_0(0)$ = centerline velocity

(V, V_1, V_2) = $(V, V_o, V_w) = (Q, Q_o, Q_w)/A$ are superficial velocities

$W(r)$ = axial velocity of PCAF

$W(1)$ = velocity of the oil/water interface in PCAF

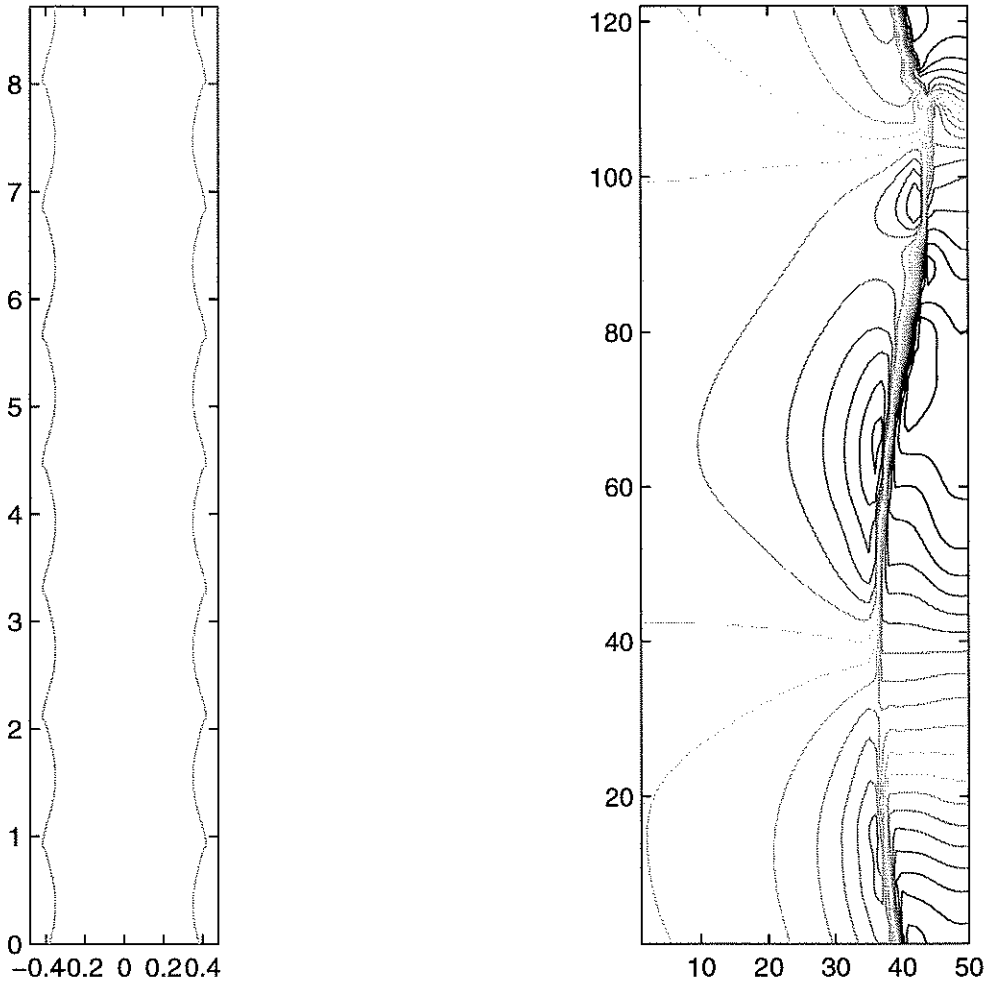

Figure 4: Up-flow with Re = 0.94983, a = 1.28, m = 0.00166, η = 1.1, J = 0.07961 and K = -0.4552. We choose the superficial oil velocity V_0 = 10.34 cms^{-1}. The wave number α is chosen as 2.0. The right figure is the contour of the pressure field corresponding to the interfacial shape.

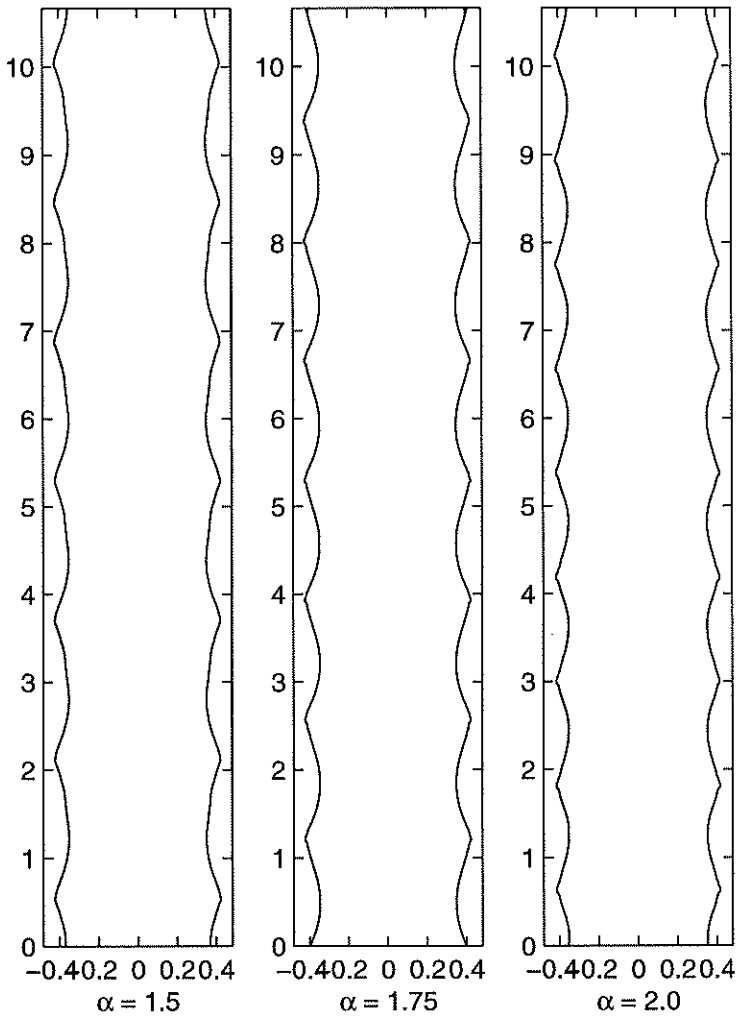

Figure 5: Up-flow for Re = 0.94983, a = 1.28, m = 0.00166, η = 1.1, J = 0.07961 and K = -0.4552. We choose different numbers of wave number α.

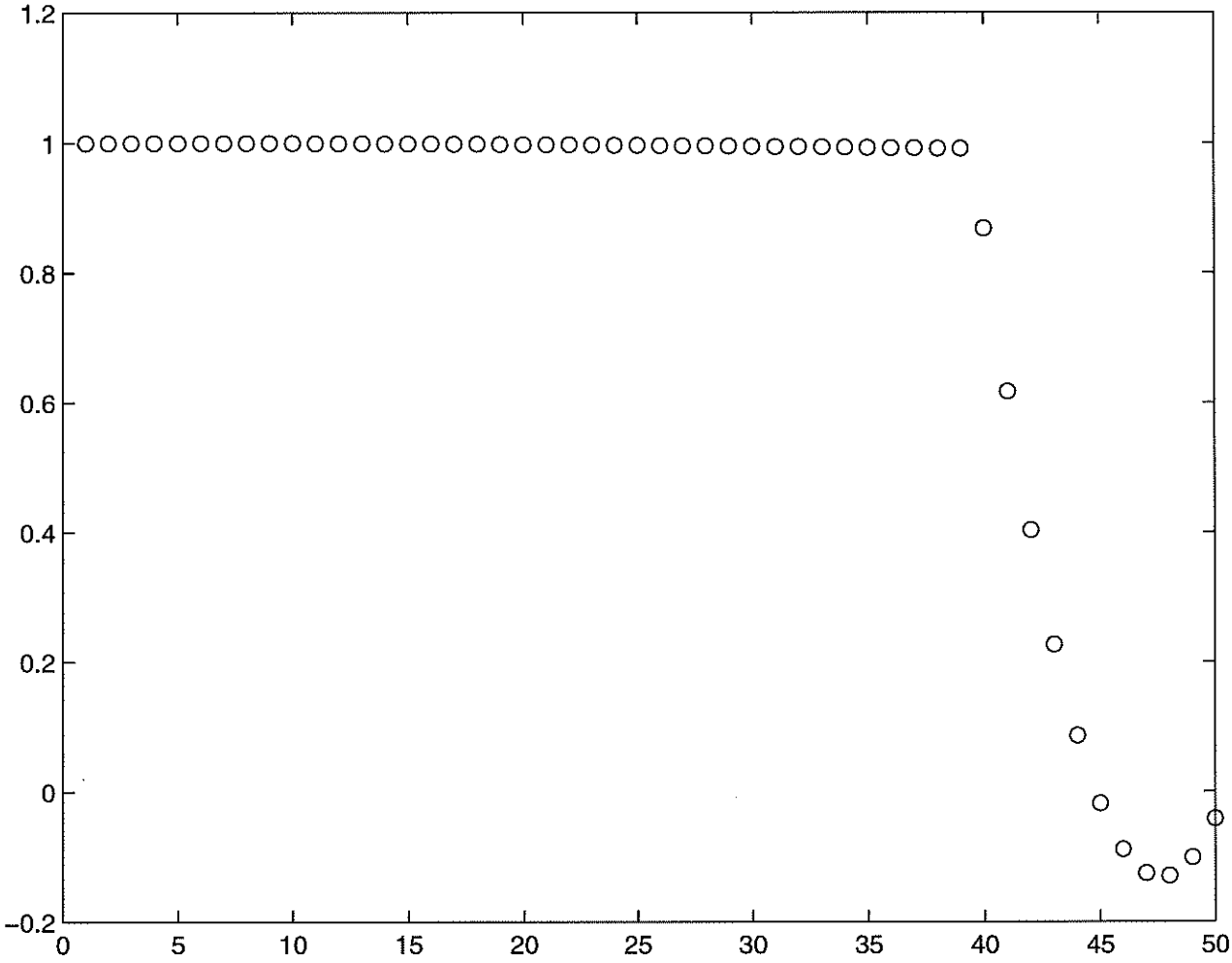

Figure 6: The mixed velocity profile for PCAF for $Re = 0.9493$, $a = 1.28$, $m = 0.00166$, $\eta = 1.1$, $J = 0.7961$ and K = -0.4552.

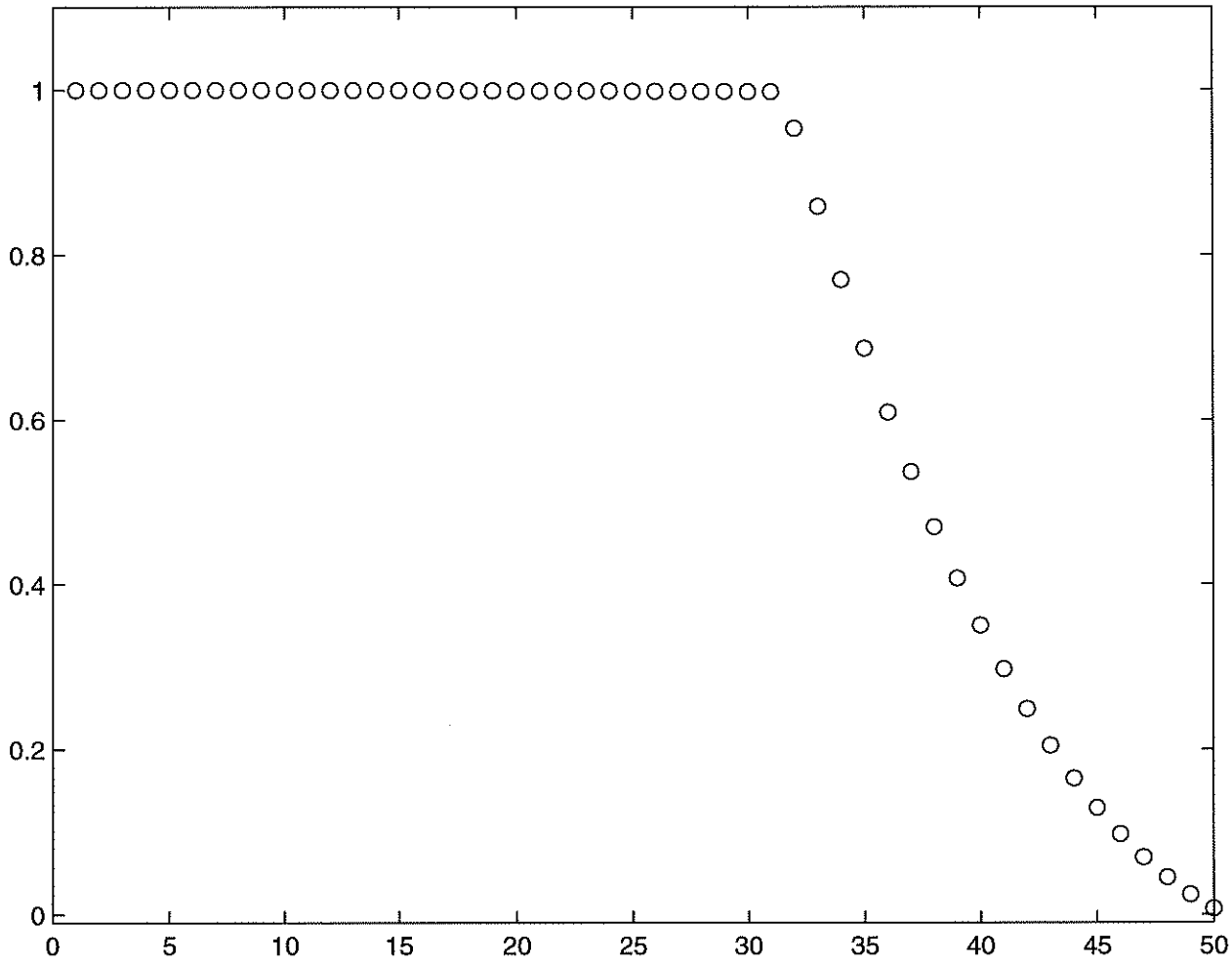

Figure 7: The up velocity profile for PCAF for $Re = 0.9493$, $a = 1.28$, $m = 0.00166$, $\eta = 1.1$, $J = 0.07961$ and K = -0.4552. The wave number α is 2.0

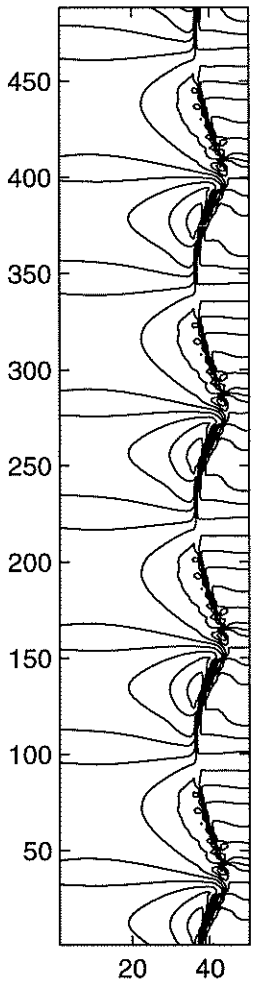

Figure 8: The contour of pressure field for PCAF for $Re = 3.0$, $a = 1.61$

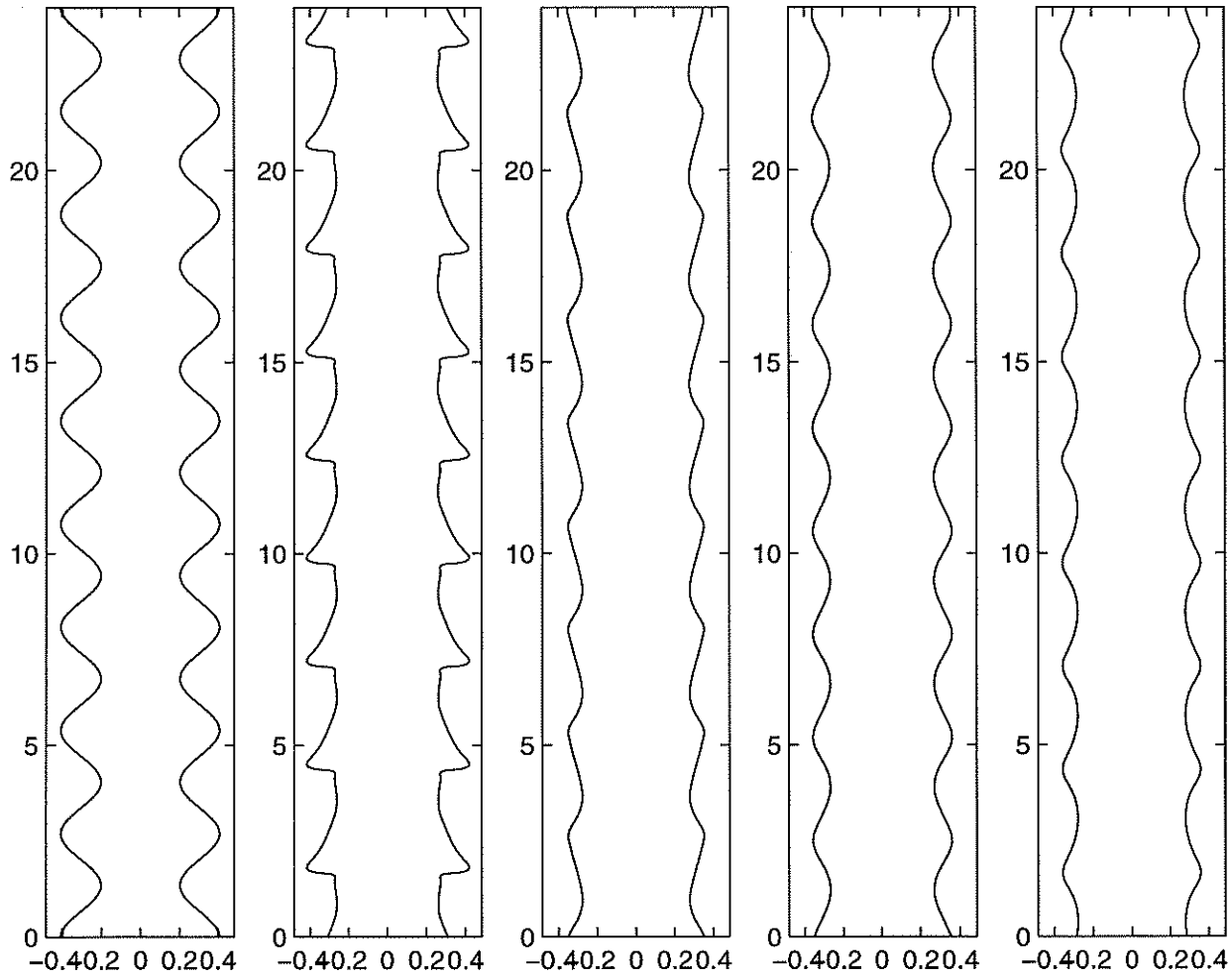

Figure 9: Interface profiles at $t = 0$, 20, 40, 60 and 140 for $Re_1 = 3.73754$, $a = 1.61$, $m = 0.00166$, $\eta = 1.1$, $J = 0.063354$ and $K =$ -2.030303. The calculation is carried out on a domain [0, 1.61] x [0, 2.618]. The wave number α is chosen as 2.4 and the initial amplitude is 0.1.

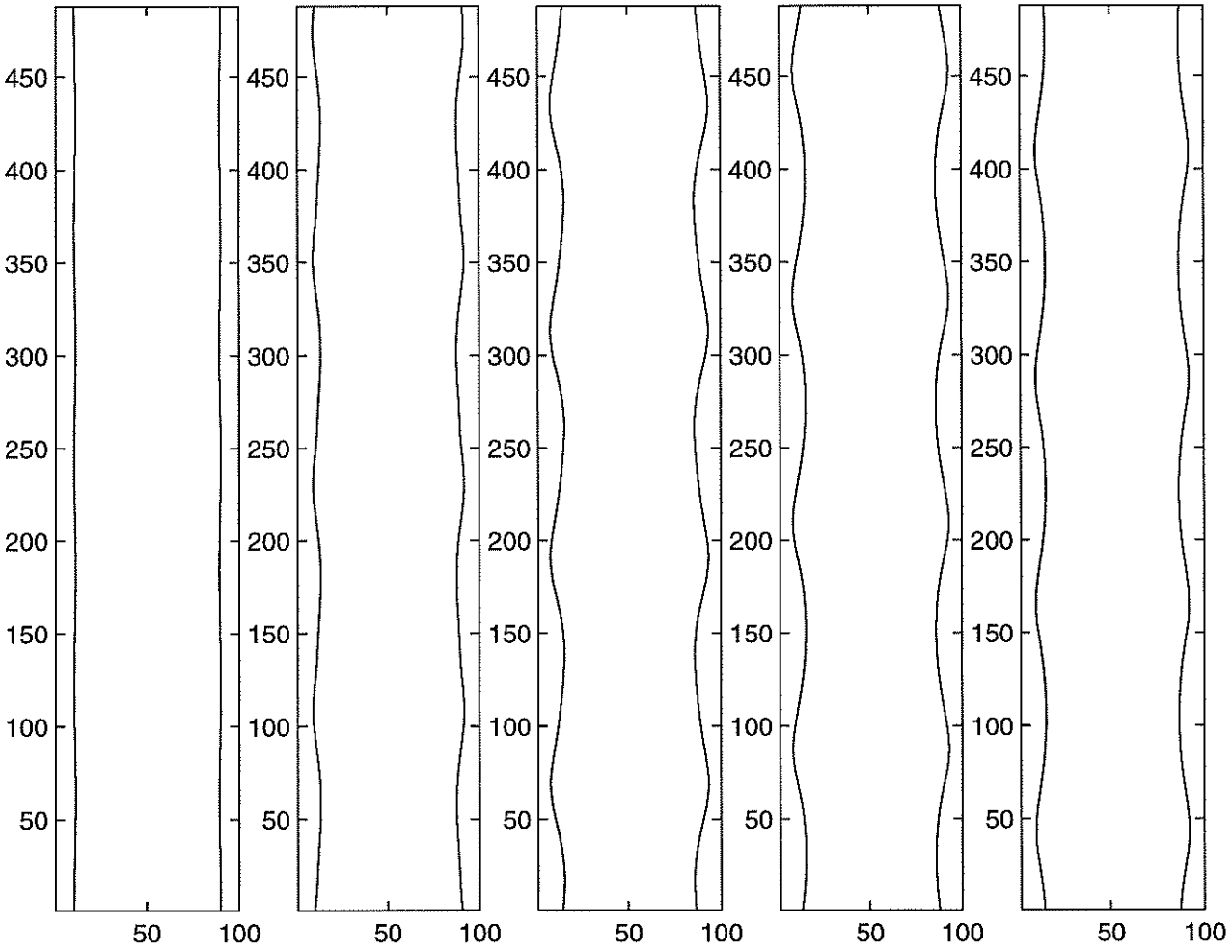

Figure 10: Up flow for $Re = 3.0$, $a = 1.28$, $m = 0.00166$, $\eta = 1.1$, $J = 0.0795$ and K = -0.9993. Our amplitude is 0.01 and wave number α is 2.0.

Figure 20: Re 2.5, case1

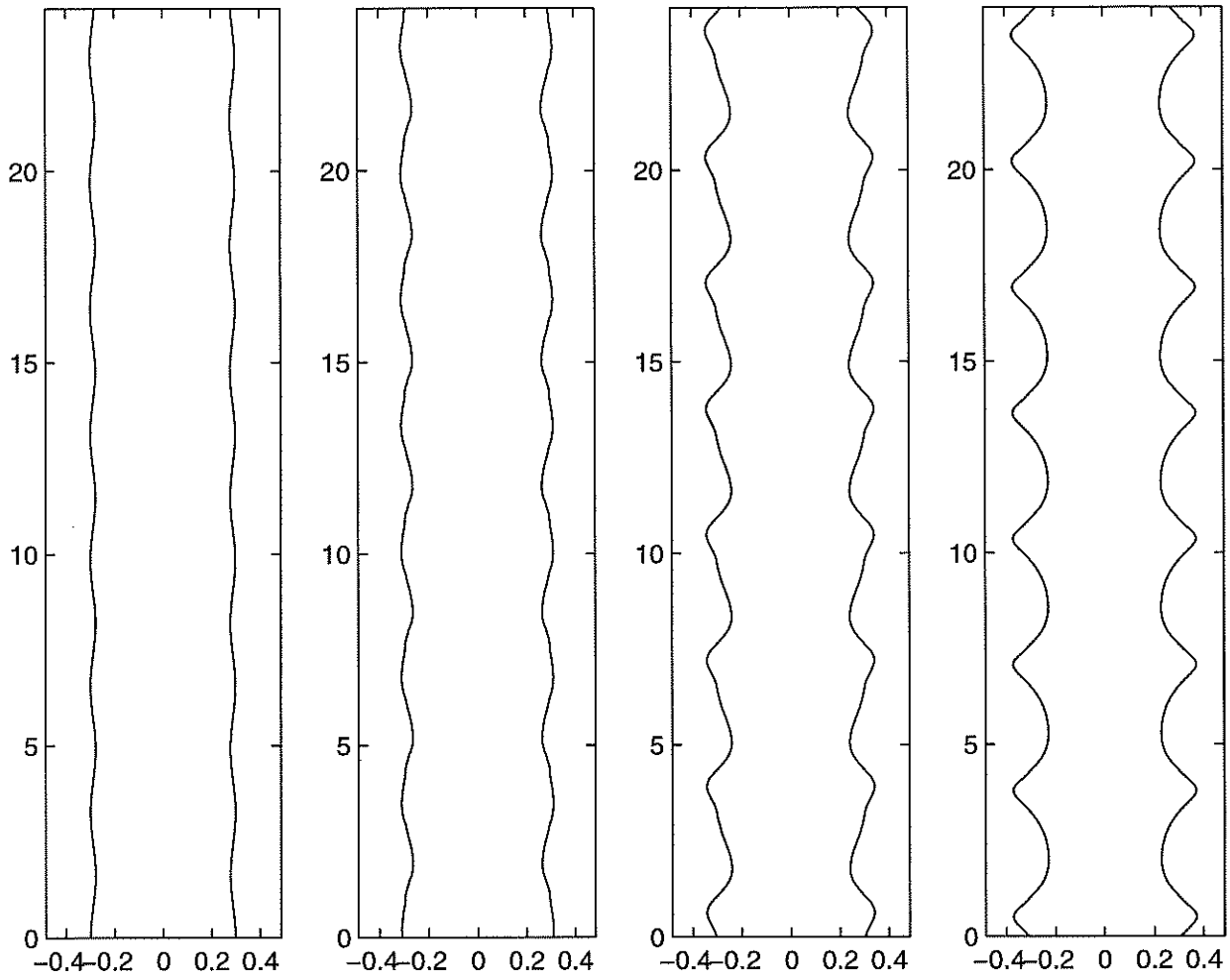

Figure 11: Down flow: Sequence of interface positions for $Re = 2.5$, $a = 1.7$, $m = 0.00166$, $\eta = 1.1$, $J = 0.06$ and K = -0.542709. Our amplitude is 0.01 and wave number α is 1.975.

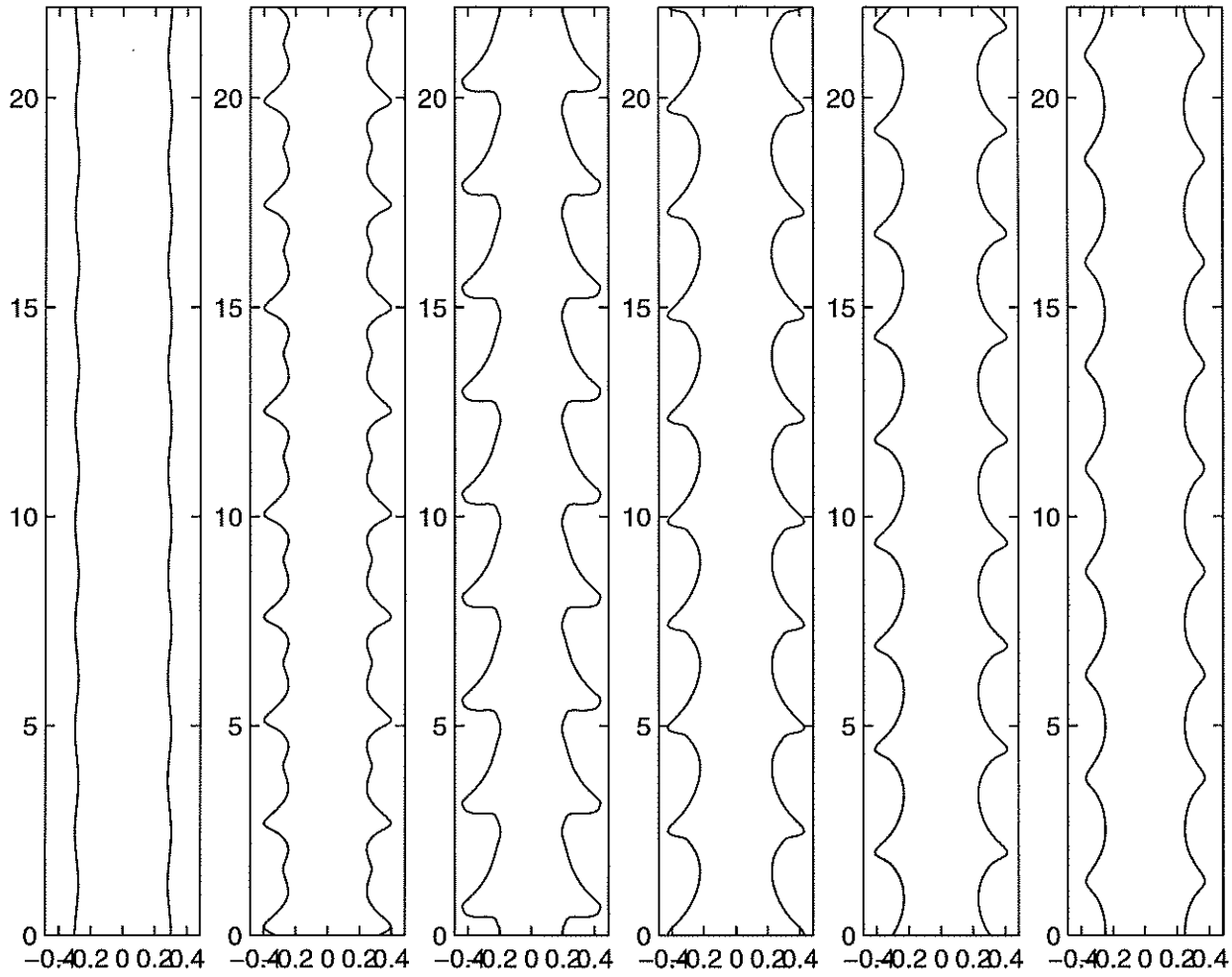

Figure 12: Down flow for $Re = 3.0$, $a = 1.7$, $m = 0.00166$, $\eta = 1.1$, $J = 0.06$ and K = -0.542709. Our amplitude is 0.01 and wave number α is 2.625.

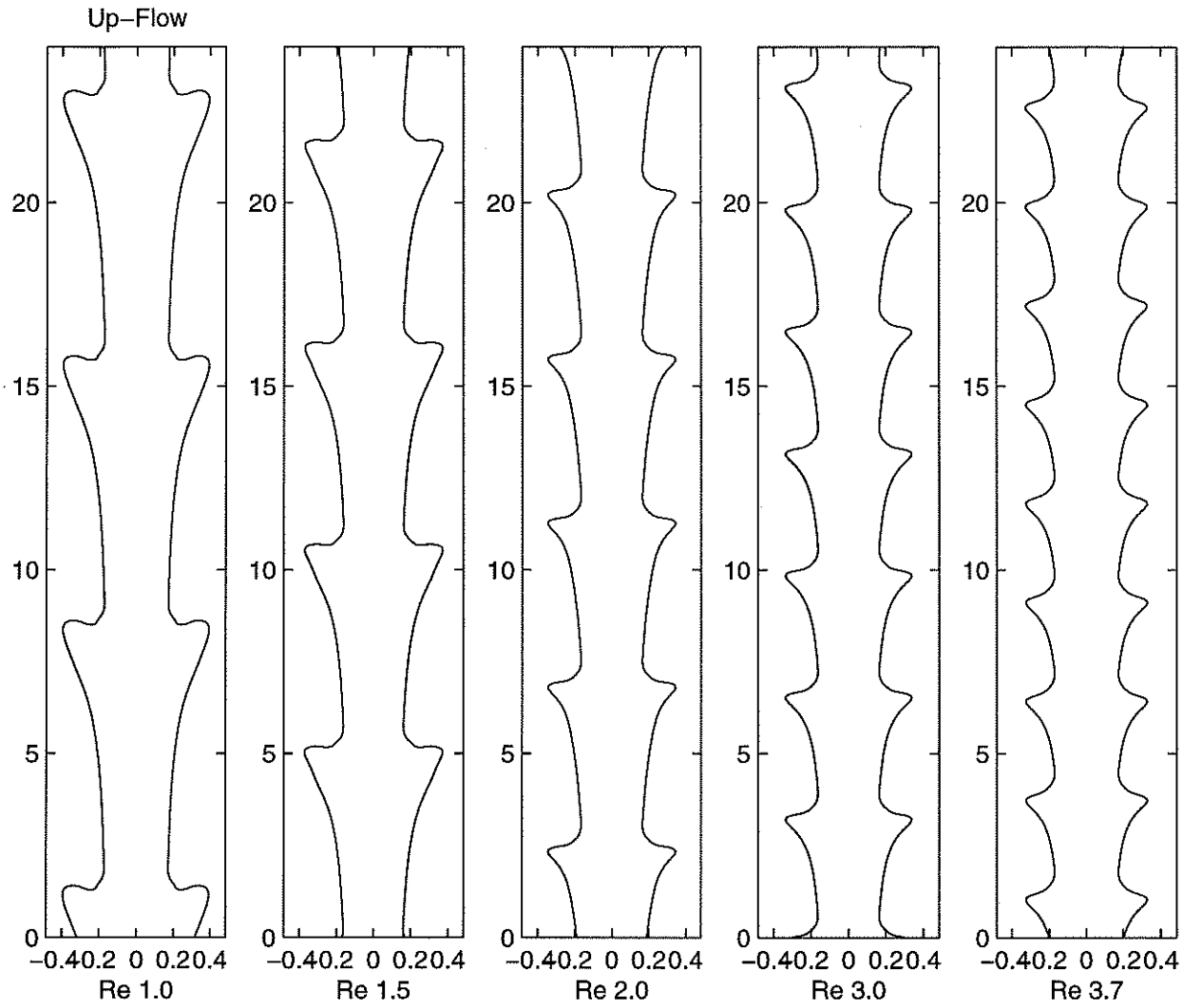

Figure 13: Up flow: $a = 1.61$, $m = 0.00166$, $\eta = 1.1$, $J = 0.0633$ and $K =$ -2.030303. Our amplitude is $A(0) = 0.02$. $Re = 1.0$, 1.5, 2.0, 3.0 and 3.7

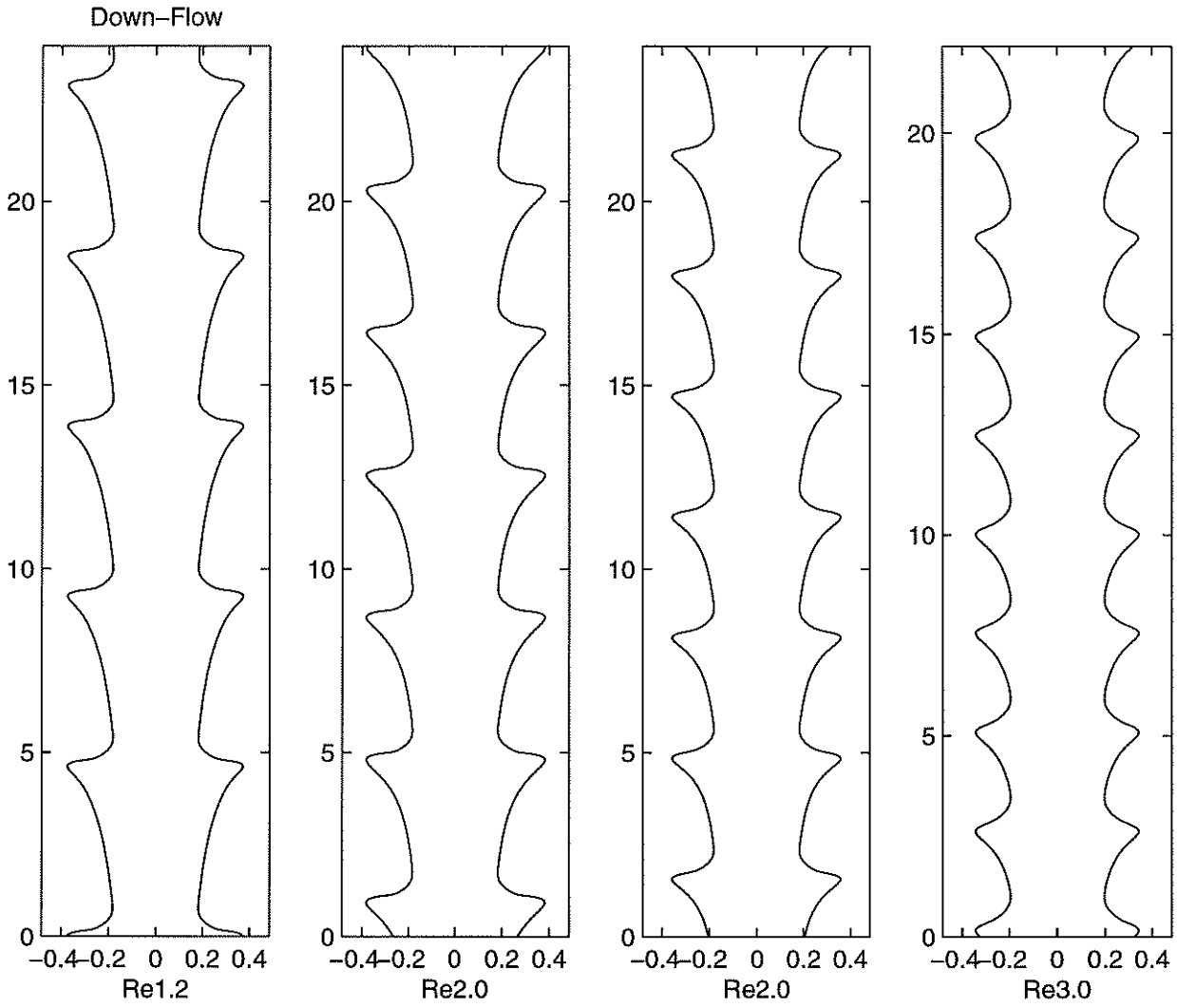

Figure 14: Down flow for $a = 1.7$, $m = 0.00166$, $\eta = 1.1$, $J = 0.06$ and K = -0.542709. Our amplitude $A(0)$ is 0.01. The Reynolds number $Re = 1.2$, 2.0, 2.5 and 3.0

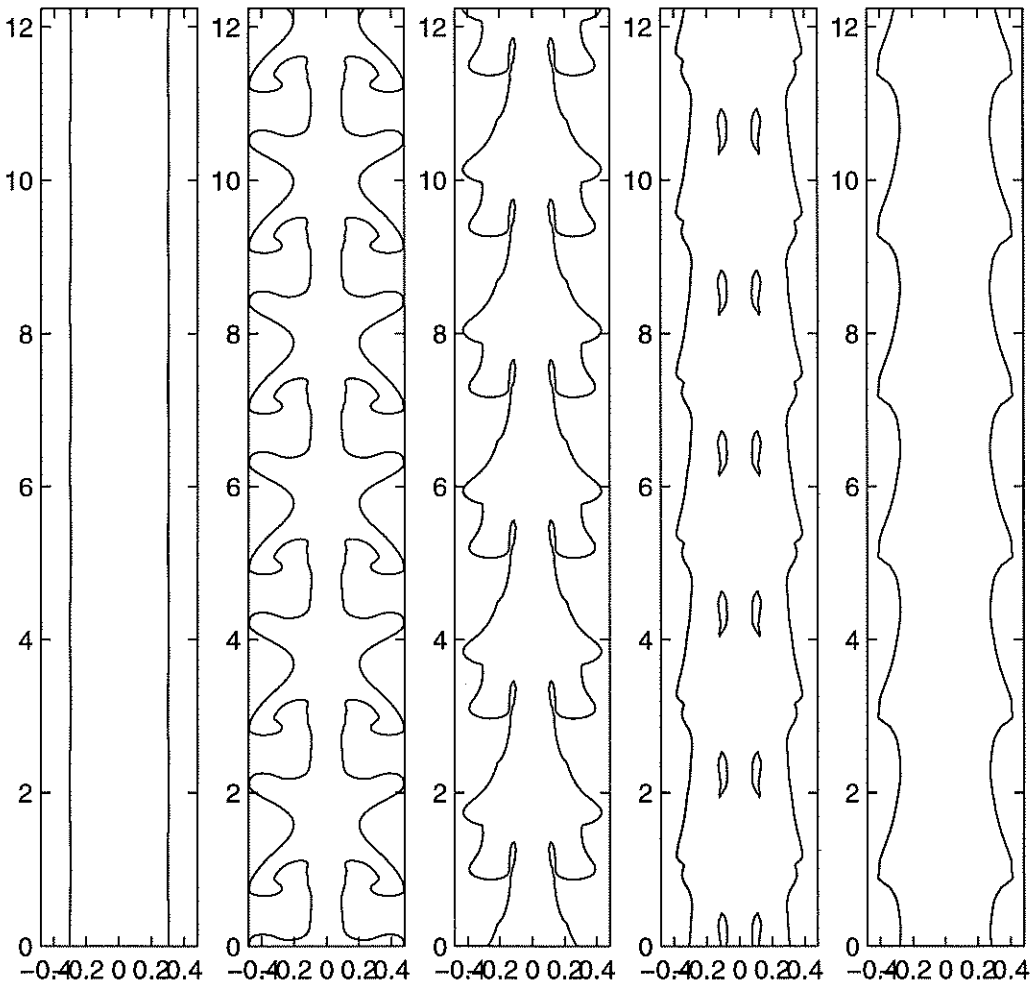

Figure 15: $Re = 1.0$, $a = 1.61$, $m = 0.00166$, $\eta = 1.1$, $J = 0.063354$ and K = -2.030303. Wave number $\alpha = 0.9$. Domain is [0, 0.47625] x [0, 6.98]

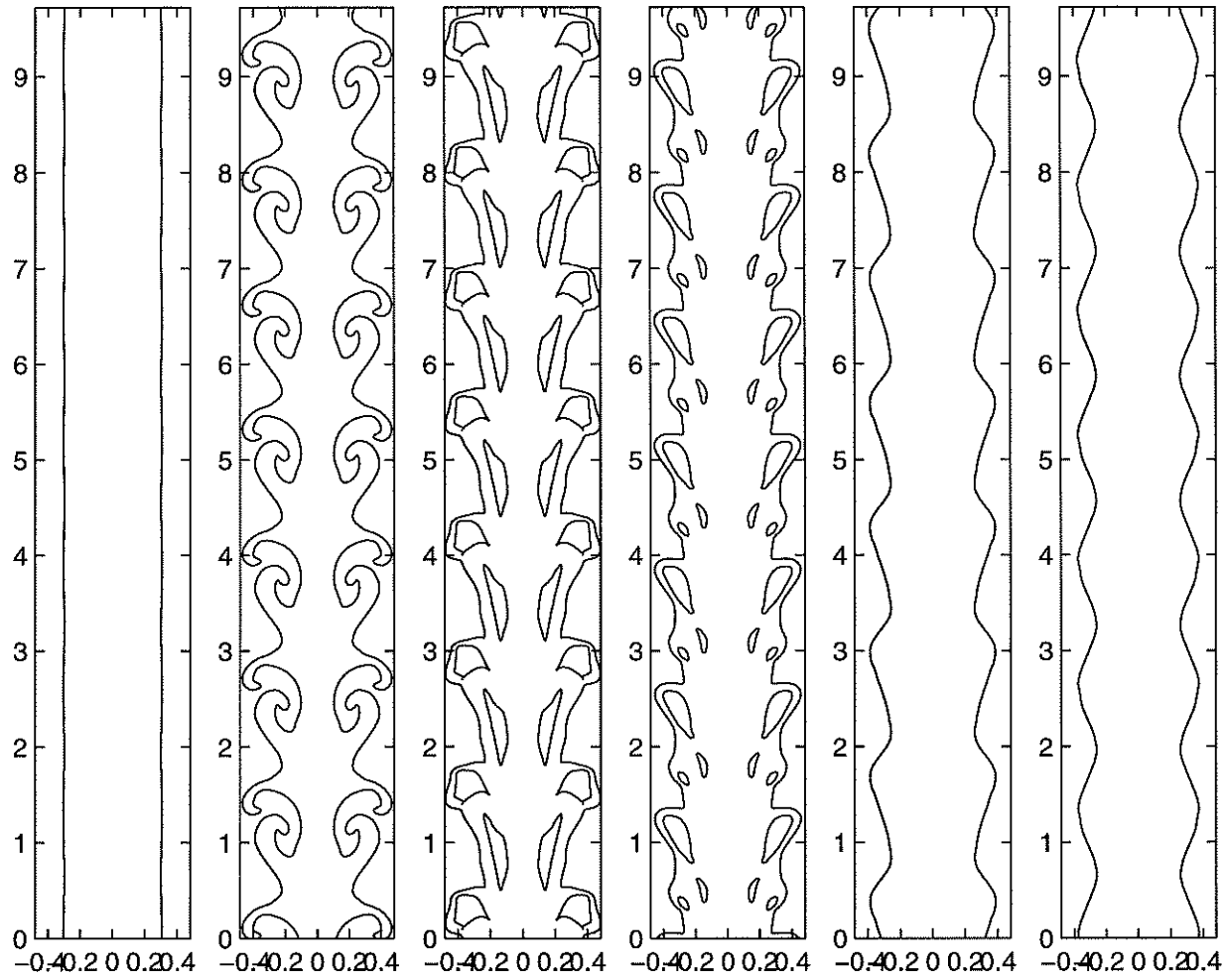

Figure 16: Vertical Flow: Re = 0.94983, a = 1.7, m = 0.00166, η = 1.1, J = 0.0796875 and K = -0.4552. Wave number is α = 3.0, final time is 1.0, domain is [-0.47625, 0.47625] x [0, 6.2832].

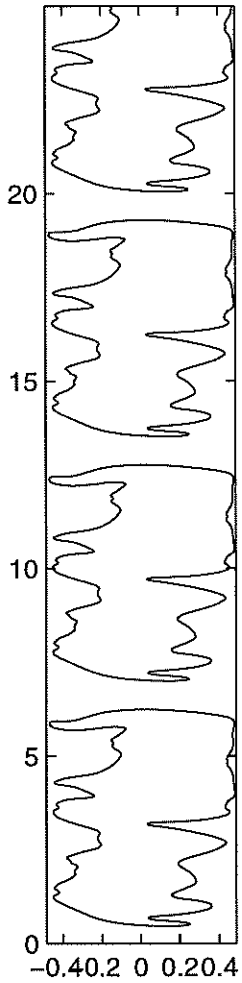

Figure 17: Vertical Flow: Re = 0.94983, a = 1.7, m = 0.00166, η = 1.1, J = 0.0796875 and K = -0.4552. Wave number is α = 3.0, final time is 1.0, domain is [-0.47625, 0.47625] x [0, 6.2832].

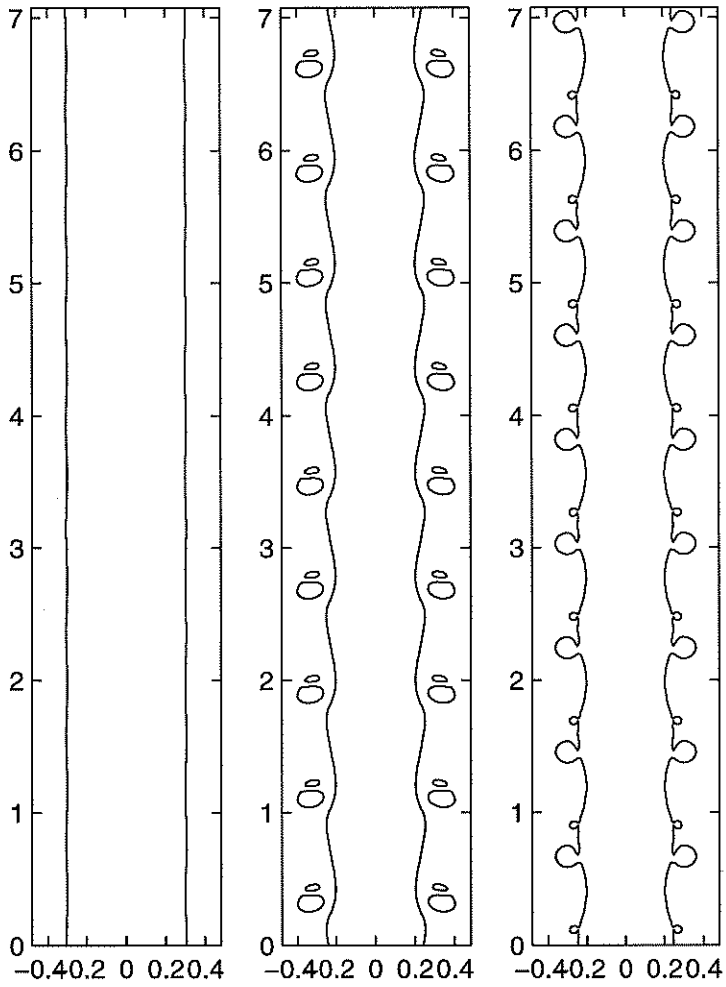

Figure 18: Vertical Flow: $Re = 3.737354$, $a = 1.61$, $m = 0.00166$, $\eta = 1.1$, $J = 0.063354$ and $K = -2.0303$. Wave number is $\alpha = 2.4$.

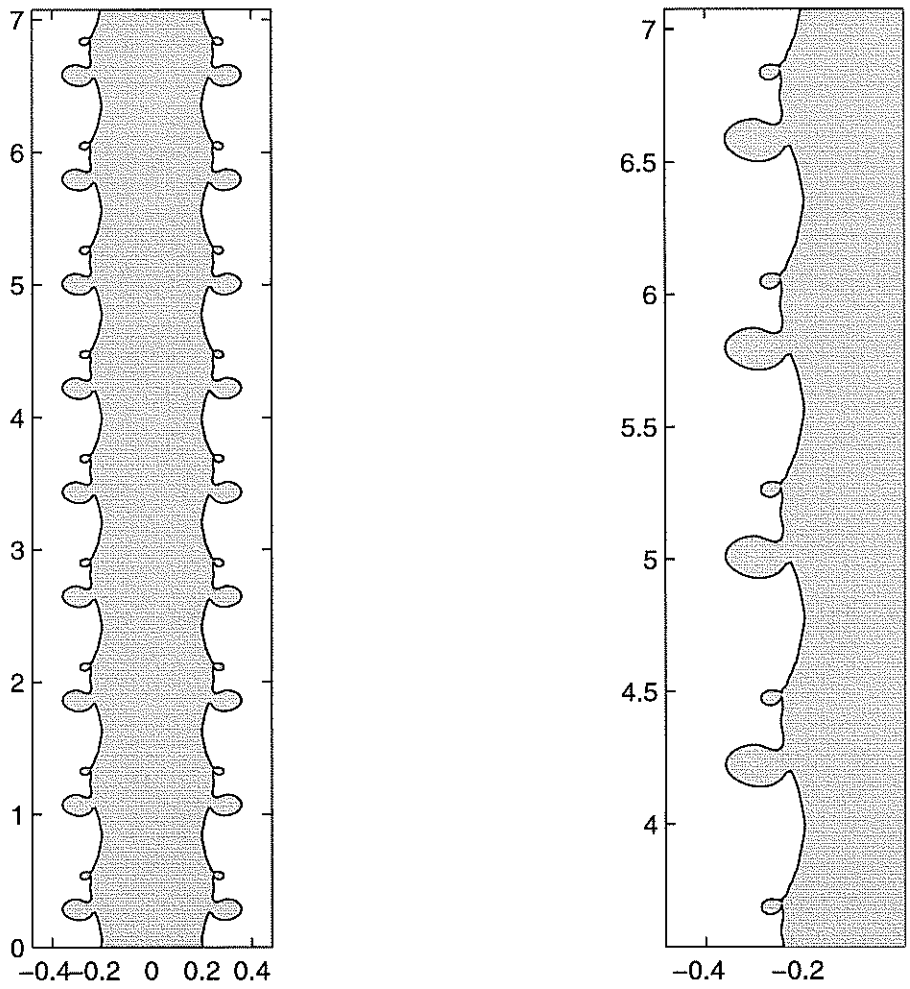

Figure 19: Zoom in the interfacial shape from Figure 18 at t = 40

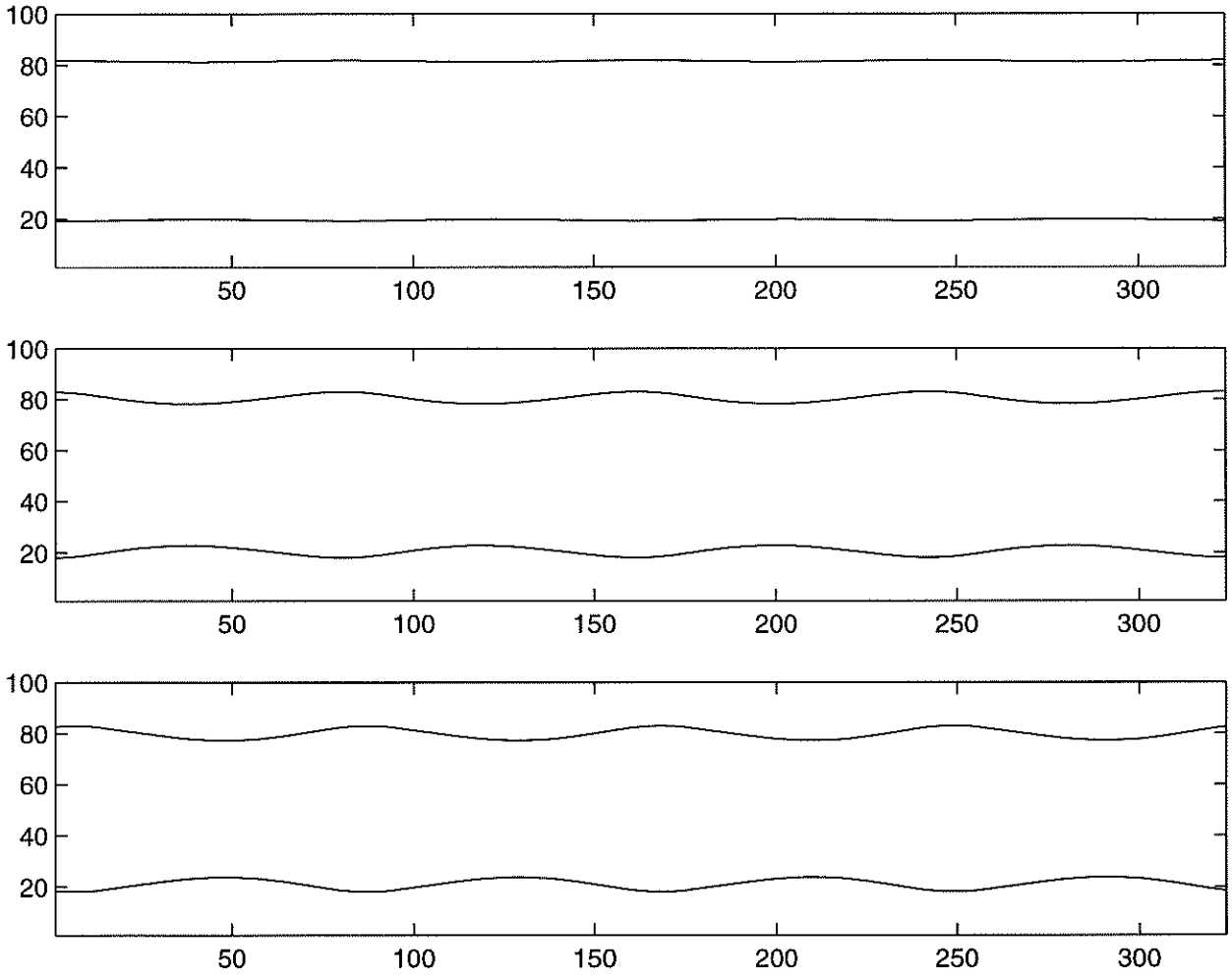

Figure 20: Simulation for Horizontal Pipe case: $Re = 3.7$, $a = 1.61$, $m = 0.00166$, $\eta = 1.1$, $J = 0.063354$ and K = -2.0303003. Wave number $\alpha = 2.4$. We use the axisymmetric property without gravity.

References

[1] R. Bai, K. Chen, and D. D. Joseph, *Lubricated Pipelining: Stability of Core-Annular Flow. Part 5. Experiments and Comparison with Theory.*, Journal of Fluid Mechanics, 240 (1992), pp. 97–142.

[2] R. Bai, K. Kelkar, and D. D. Joseph, *Direct Simulation of Interfacial Waves in a High Viscosity Ratio and Axisymmetric Core Annular Flow*, Journal of Fluid Mechanics, 327 (1996), pp. 1–34.

[3] J. U. Brackbill, D. B. Kothe, and C. Zemach, *A Continuum Method for Modeling Surface Tension*, Journal of Computational Physics, 100 (1992), pp. 335–353.

[4] Y. C. Chang, T. Y. Hou, B. Merriman, and S. Osher, *A Level Set Formulation of Eulerian Interface Capturing Methods for Incompressible Fluid Flows*, Journal of Computational Physics, 124 (1996), pp. 449–464.

[5] A. J. Chorin, *Numerical Solution of the Navier-Stokes Equations*, Math. Comp, 22 (1968).

[6] A. V. Coward, Y. Y. Renardy, M. Renardy, and J. R. Richards, *Temporal Evolution of Periodic Disturbances in Two-Layer Couette Flow*, Journal of Computational Physics, 132 (1997), pp. 346–361.

[7] C. W. Hirt and B. D. Nichols, *Volume of Fluid (VOF) Method for the Dynamics of Free Boundaries*, Journal of Computational Physics, 39 (1981), pp. 201–225.

[8] D. D. Joseph, *Stability of Fluid Motions I, II*, Springer-Verlag, 27 and 28 (1976).

[9] D. D. Joseph, R. Bai, K. P. Chen, and Y. Y. Renardy, *Core Annular Flows*, Annual Review of Fluid Mechanics, 29 (1997), pp. 65–90.

[10] D. D. Joseph and Y. Y. Renardy, *Fundamentals of Two-Fluid Dynamics, Part I, Mathematical Theory and Applications; Part II, Lubricated Transport, Drops and Miscible Liquids*, Springer-Verlag, New York, (1993).

[11] D. D. JOSEPH AND D. G. SCHAEFFER, *Two Phase Flows and Waves*, The IMA Volumes in Mathematics and Its Applications, 26 (1989), pp. 98–117.

[12] M. KANG, *private communication.*

[13] M. KANG, R. P. FEDKIW, AND X.-D. LIU, *A Boundary Condition Capturing Method for Multiphase Incompressible Flow*, UCLA, CAM Report, (1999).

[14] J. LI AND Y. Y. RENARDY, *Direct Simulation of Unsteady Axisymmetric Core-Annular Flow with High Viscosity Ratio*, preprint, (1998).

[15] J. LI, Y. Y. RENARDY, AND M. RENARDY, *A Numerical Study of Periodic Disturbances on Two-Layer Couette Flow*, Physics of Fluids, 10 (1998), pp. 3056–3071.

[16] W.-H. LI AND S.-H. LAM, *Principles of Fluid Mechanics*, Addison-Wesley, (1964).

[17] B. J. MILLER, *Improvements in Computing Multiple Phase Flows*, PhD thesis, University of California, Los Angeles, 1997.

[18] G. OOMS, A. SEGAL, AND S. CHEUNG, *Propagation of Long Waves of Finite Amplitude at the Interface of two viscous Fluids*, International Journal of Multiphase Flow, 11 (1985), pp. 485–502.

[19] S. OSHER AND J. A. SETHIAN, *Fronts Propagating with Curvature-Dependent Speed : Algorithms Based on Hamilton-Jacobi Formulations*, Journal of Computational Physics, 79 (1988), pp. 12–49.

[20] S. OSHER AND C.-W. SHU, *High-Order Essentially Non-Oscillatory Schemes for Hamilton-Jacobi Equation*, SINUM, 28 (1991), pp. 907–922.

[21] D. PENG, B. MERRIMAN, S. OSHER, H. K. ZHAO, AND M. KANG, *A PDE Based Fast Local Level Set Method*, Journal of Computational Physics, 55 (1999), pp. 410–438.

[22] R. PEYRET AND T. D. TAYLOR, *Computational Methods for Fluid Flow*, Springer-Verlag, (1990).

[23] Y. Y. RENARDY, *Snakes and Corkscrews in Core-Annular Down-flow of Two Fluids*, Journal of Fluid Mechanics, 340 (1997), pp. 297–317.

[24] C.-W. SHU AND S. OSHER, *Efficient Implementation of Essentially Non-Oscillatory Shock Capturing Schemes, II*, Journal of Computational Physics, 83 (1989), pp. 32–78.

[25] M. SUSSMAN, E. FATEMI, P. SMEREKA, AND S. OSHER, *A Level Set Approach for Computing Solutions to Incompressible Two-Phase Flow II*, CAM Report, 83 (1998).

[26] M. SUSSMAN, P. SMEREKA, AND S. OSHER, *A Level Set Method of Computing Solutions to Incompressible Two-Phase Flow*, Journal of Computational Physics, 119 (1994), pp. 146–159.

[27] J. N. TSITSIKLIS, *Efficient Algorithms for Globally Optimal Trajectories*, IEEE Transactions on Automatic Control, 40 (1995), pp. 1528–1538.

[28] S. O. UNVERDI AND G. TRYGGVASON, *A Front-Tracking Method for Viscous, Incompressible, Multi-Fluid Flows*, Journal of Computational Physics, 100 (1992), pp. 25–37.